Review on Theoretical Models of Void Evolution in Crystalline Particles

S.A. Krasnitckii[1,2,3], M.Yu. Gutkin[1,2,3]

[1] ITMO University, Kronverkskii pr. 49, St. Petersburg, 197101, Russia
[2] Institute for Problems in Mechanical Engineering, Russian Academy of Sciences, Bolshoi 61, Vasil. Ostrov, St. Petersburg, 199178, Russia
[3] Peter the Great St. Petersburg Polytechnic University, Polytekhnicheskaya 29, St. Petersburg, 195251 Russia

Abstract. In the review, the up-to-date theoretical research of various aspects of void evolution problem in hollow crystalline micro- and nanostructures is summarized. A classification of hollow architectures of micro- and nanostructures distinguishing the main procedures of void (pore) production as well as the influence of the voids on functional properties of the devices based on hollow structures, is suggested. The factors responsible for the void evolution process are discussed. Finally, theoretical models of the void evolution describing shrinkage and growth processes in particles of various structures are considered in terms of kinetics and thermodynamics concepts.

ABBREVIATIONS

SCP   single-crystalline particle
PCP   polycrystalline particle
CShP   core-shell particle
MTP   multiply twinned particle
PW   pentagonal whisker or wire
DhP   decahedral particle
IcP   icosahedral particle
WD   wedge disclination
SD   stereo disclination (or Marks-Ioffe disclination)
TEP   thermodynamic extremal principle
FCC   face-centered cubic

NOTATIONS

r spherical or cylindrical radial coordinate
r_i, r_e internal and external radii of a hollow particle
r_f radius of a solid particle
C_v relative concentration of the vacancies
D_v vacancy diffusivity

$\mathbf{j}_c$ vacancy flux caused by concentration gradient
$\mathbf{j}_\sigma$ vacancy flux caused by intrinsic stress field
Ω atomic volume
δv relaxation volume
γ specific surface energy
σ_h hydrostatical stress
ω strength of partial wedge disclination
χ strength of stereo (Marks-Ioffe) disclination
E Young modulus
μ shear modulus
ν Poisson coefficient

1. INTRODUCTION

In the last two decades, there has been an increasing interest in development of theoretical models describing the void evolution kinetics in micro- and nanostructures of different architectures. This interest is encouraged by extended experimental investigations of hollow structures and their synthesis, as well as by elucidation of unique functional properties of the

Corresponding author: S.A. Krasnitckii, e-mail: krasnitsky@inbox.ru

hollow crystalline objects against their solid counterparts. This article is mainly aimed at reviewing the issues concerning theoretical aspects of hollow micro- and nanostructures production.

1.1. Classification

The variety of hollow crystalline structures can be categorized in terms of particle morphology, shell and cavity architecture, material composition and structural complexity [1,2]. For instance, the hollow particles often take the form of hollow sphere, tube, box and other hollow polyhedral shapes with well-defined facets (Fig. 1a–c). Besides, porous hollow particles with large through-holes and hollow polyhedra with frame-like or cage-like open architectures can be incorporated in special class of hollow particles with open structures (Fig. 1d). Torus or ring particles with different cross sections can be also attributed to hollow particles with open structures (Fig. 1e). Considering the shell architectures, hollow particles can be classified as single-shell, double-shell or multi-shell particles (Fig. 1f,g). The hollow structures with interior cavity comprising solid particles arrange the class of rattle-type hollow structures including yolk-shell particles which contain one solid core inside the shell (Fig. 1h). Concerning the hollow architectures (complexity), particles can contain single or multiple

cavities (Fig. 1j). Crystalline hollow structures can be considered in terms of material composition ranging from pure element to multicomponent systems, and from metals to semiconductors. Hierarchical hollow structures are more complicated structures which are usually assembled of solid subunits such as nanoparticles, nanorods or nanosheets. From the theoretical point of view, spherical and cylindrical geometries of hollow structures are the most appropriate for analyzing void evolution processes.

1.2. Functional properties

Determined by high specific area and surface-to-volume ratio, low density and encapsulate option, hollow structures exhibit higher performance than their solid counterparts with the same composition and size that tremendously extends their application in the fields of plasmonics [3–5], catalysis [6–11], energy storing [12–15] and medicine [16–18].

For instance, hollow metal nanoparticles have significantly higher *plasmonic properties* than their solid counterparts due to so-called mechanism of plasmon hybridization. An ability to generate a surface plasmonic resonance within a wide energy range from ultraviolet to near infrared regions by tunning of void size was numerically proved by the Mie scattering calculations on the 50 nm hollow spherical Ag and Au
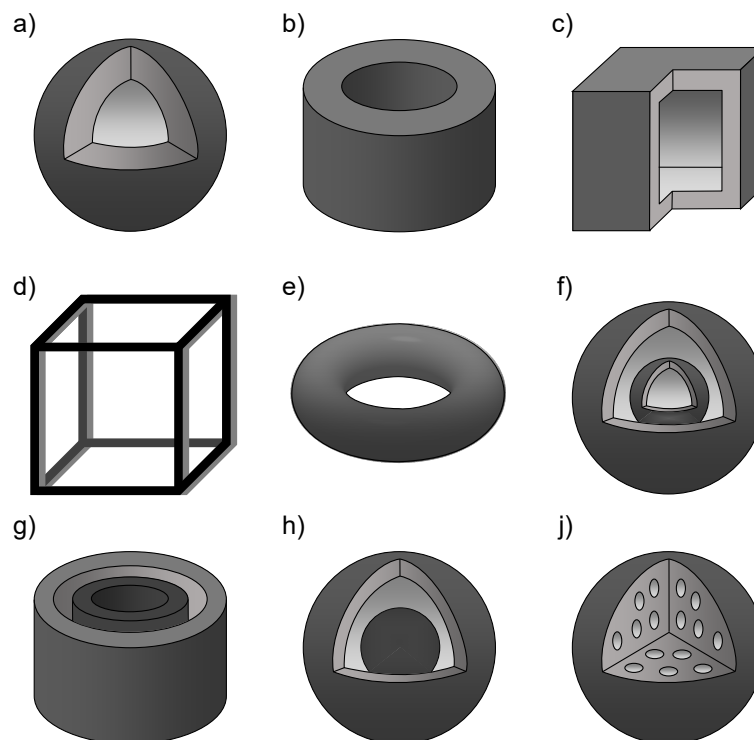
Fig. 1. Sketches showing the diversity of hollow particles: a) spherical; b) tubular; c) cubic; d) frame-like; e) torus; f), g) multi-shell; h) yolk-shell; j) porous.

nanoparticles with different shell thickness [19]. This tunability of surface plasmonic resonance makes the metal hollow particles a promising material for gas sensing [20–22], surface enhanced Raman spectroscopy [23–25], plasmon enhanced solar cells [26–28], photodetectors [29–31], drug delivery [32,33] and cancer therapy [34–36].

Hollow semiconductor particles exhibit more improved *photocatalytic activity* than solid ones due to shortened diffusion pathways of the electron-hole pairs as well as better capacity to accelerate the surface reactions [37–40]. Besides, the multiple reflection of light and its scattering inside the hollow interior can envisage stronger light absorption and enhanced light-harvesting capability.

Due to higher fraction (abundance) of surface sites, hollow metal particles (with alloy and core-shell structures) enhance *electrocatalytic* activities in reactions of oxygen reduction, oxygen evolution, hydrogen evolution, and hydrogen oxidation making these particles perfect candidates for industrial scale of proton-exchange membrane fuel cell technology and other industrial applications [41–45].

The hollow carbon or metal oxides structures as materials for anodes [46,47], cathodes [48,49] and electrodes [50,51] benefit from the high active surface area to enhance capacity of *energy storage* devices, such as batteries and supercapacitors. Besides, presence of voids reduces the volumetric strain in hollow structures that increases the cycling stability of the devices.

Thus, fabrication of hollow structures with designed functional properties is significant issue requiring both a choice of suitable synthesis procedures (optimal synthesis conditions) and a creation of theoretical models describing the kinetics of void evolution processes in particles of different nature.

1.3. Synthesis procedures

Generally, the template-based strategies are usually employed to classify the synthesis procedures of hollow structures [52–58].

Hard-templating strategy is the most trivial (conventional) tool for synthesis of hollow nanostructures. A wide range of materials such as polymer, silica, carbon, metal ceramic, inorganic salts, and natural materials can be employed as the base for hard templates. According to this strategy, the surface of a hard template is covered with shell layer of desired material. The hollow nanostructures can be obtained by the selective removal of hard template through the well-known techniques such as chemical etching,

temperature treatment (calcination) or dissolving in solvents. The resulted shape of hollow nanostructures (hollow sphere, tube, box, etc.) is completely determined by the original shape (spherical, cylindrical, cubic) of the hard template, replicating its morphology.

Soft-templating strategy employs fluid or gas substances as templates (such as emulsion droplets, vesicles/micelles, gas bubbles) to synthesize the hollow nanostructures avoiding the stage of post (treatment) removal of templates, in contrast to the above-mentioned (hard template) strategy. This strategy is also applicable to fabricate the complicated hierarchical hollow structures such as porous spherical shells, hollow spheres with vesicular buds, etc. However, soft-template strategy is not suitable for the synthesis of non-spherical hollow structures with sharp edges and corners. Besides, the synthetized hollow structures have a high diversity (scatter) in the size distributions of both particle and interior cavity that makes it difficult to control uniformity.

Self-templating strategy is considered as more advantageous for synthesis of hollow nanostructures in terms of relatively simple procedure, high reproducibility, and size parameter control. According to this strategy, the hollow nanostructure is produced on the basis of the original solid nanostructure as a template employing the following mechanisms: the Ostwald ripening, the nanoscale Kirkendall effect, galvanic replacement, etc. Hollowing process through the *Ostwald ripening* mechanism in nanostructures occurs due to the fact that the smaller voids have a tendency to dissolve and subsequently regrow in bigger ones. Generally, this mechanism can be applied to structures made from crystalline materials as well as polymeric. As another mechanism of self-templating approach, the nanoscale *Kirkendall effect* has been widely employed for production of hollow particles (mainly metal oxides) [59,60]. For instance, the nanoscale Kirkendall effect occurs in the core-shell particle with fast diffusive component in the core and relatively slow diffusive component in the shell. Under these conditions, the difference in diffusion rates of components induces the outward imbalanced flux of matter. This flux has to be compensated by the inward flux of vacancies, which can lead to vacancy supersaturation in the interior region and subsequent formation of voids. Hollowing process via *galvanic replacement reaction* is driven by electrochemical (reduction) potential difference between two metals [61]. According to this classical mechanism, the redox reaction between salt of more noble metal (B) and a core of less noble metal (A) results in both deposition of (B) atoms on the core surface due to reduction process and dissolution of (A) core due to
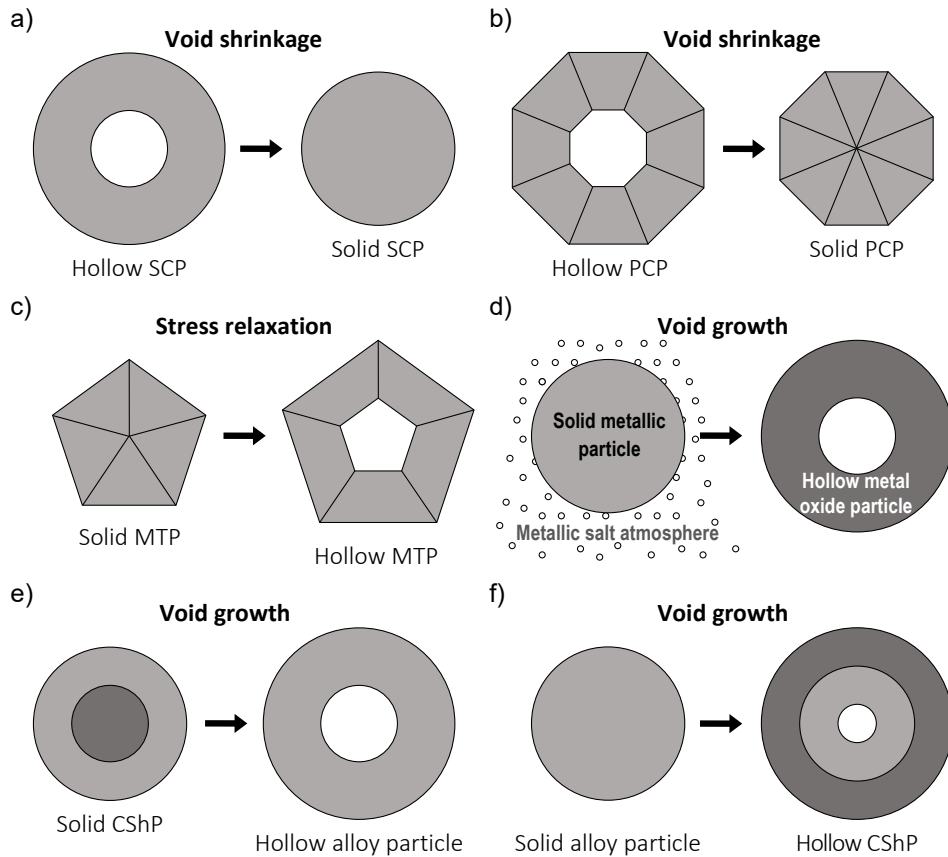
Fig. 2. Void evolution phenomena in particles: a) void shrinkage in a single-crystalline particle (SCP); b) void shrinkage in a polycrystalline particle (PCP); c) residual stress relaxation due to the void formation in a multiply twinned particle (MTP); d) void growth in a metallic particle due to oxidation in surrounding atmosphere; e) void growth in a core-shell particle (CShP) due to the Kirkendall effect; f) void growth in an alloy particle due to the phase separation.

oxidation process. The final shape and size of alloyed shell are strongly determined by (A) core. For relatively long reaction times, the generation of multiple pores occurs in the shell, which eventually leads to the formation of cage and frame structures.

Although a large number of reviews has been devoted to various aspects of synthesis of hollow nanostructures as well as the influence of hollows on the functional properties of the devices based on hollow nanostructures, not enough information is available on the theoretical aspects of hollow formation. By referring to the previous theoretical solutions, this article provides substantial review on theoretical models of hollow formation in nanostructures.

1.4. Phenomena of void evolution in particles

The process of void evolution is driven by different factors including particle environment and size [62,63], structural crystallinity [64], diffusivity of components [65,66], presence of vacancy sinks/ sources (such as dislocations, disclinations, grain and interface boundaries) [67–69], surface and volume stress states [70–73].

By now, the following phenomena of void evolution in nanoparticles have been theoretically described in detail:

(i) void shrinkage in initially hollow particles with single crystalline (Fig. 2a) and polycrystalline structures (Fig. 2b). This phenomenon is driven by Gibbs-Thompson curvature effect concerning the difference of vacancy concentration on the curvature surfaces from the equilibrium one on the planar surfaces;

(ii) void formation in multiply twinned particles (MTPs) induced by the residual stress relaxation (Fig. 2c). MTPs are attributed to high level of residual stress induced by five-fold cycling twinning. This stress state can relax through various channels such as formation of dislocation loops, cracks, mismatched layers and particularly voids;

(iii) void growth in initially solid metal nanoparticles of pure element due to oxidation reaction in O, S, Se, Te, N, or P surrounding atmosphere (Fig. 2d). According to this phenomenon, solid metal particles during oxidation turn into hollow sulfide, selenide, phosphide, etc. particles through the nanoscale Kirkendall effect. The thin oxide shells occur with subsequent diffusion of metal atoms toward the external particle surfaces. Outward diffusion of metal atoms drives the void formation, resulting in hollow or porous particles;

(iv) void growth in initially solid nanoparticles of binary component element accompanied by both phase transformation (Fig. 2e) and separation (Fig. 2f). These phenomena are driven by nanoscale Kirkendall effect as well. In the first case, the faster diffusing species should be located in the core while the slower diffusing species form the shell (Fig. 2e).

Although these phenomena are widely referenced in literature, there is a lot of issues to elucidate. This review is an attempt to summarize main results of theoretical researches in the field of void evolution kinetics in both crystalline micro- and nanoparticles to create a snapshot of the current understanding of these phenomena.

1.5. Context of this review

By now several excellent overviews [74–78] summarizing the results of theoretical analysis of void evolution kinetics in hollow particles are available. However, these reviews do not include the state-of-the-art models of void evolution in hollow particles. Concerning the rapid development of nanotechnology, we believe that this Review would serve not only as theoretical overview of recent progress in the field but also as a kind of recommendation for choice of synthesis conditions for experimentalists.

2. VOID SHRINKAGE PHENOMENA IN HOLLOW PARTICLES

Voids in hollow single-crystalline particles (SCPs) of pure elements are unstable and have a tendency to shrinkage in a compact particle. The physical mechanism of this phenomenon is attributed to vacancy diffusion flux from the inner surface to the outer one driven by the vacancy concentration gradient between the particle surfaces (so called Gibbs-Thompson curvature effect). Besides, the void shrinkage should be advantageous pathway in terms of energy balance as a result of surface energy reduction.

The void shrinkage phenomenon in hollow compound particles was verified experimentally [79–83].

Nakamura et al. [79] was the first who investigated the phenomenon of void shrinkage and collapse in NiO and Cu_2O oxide nanoparticles while annealing in air with transmission electron microscopy (TEM). As a result, the oxide particles transformed into solid metallic Cu and Ni nanoparticles due to shrinking associated with the reduction reaction. Besides, Nakamura et al. [80] studied the stability of hollow oxide nanowires produced by the oxidation reaction. Nanotubes exhibited a tendency to shrink into solid oxide nanowires after heating to sufficiently high temperatures. Slow shrinkage process of Ag/Au and Ag/Pd hemispherical core-shell structures at temperatures higher than the formation temperature was observed by Glodán et al. [81]. Void collapse of NiO nanoparticles due to chemical reduction was also reported in [82,83].

Void shrinkage phenomenon was also established numerically by Monte-Carlo atomistic simulations of SCP [84,85] and molecular dynamic simulations for both single-crystalline [86–89] and polycrystalline [90–92] nanoparticles. Gusak et al. [84] employed Monte-Carlo simulation to confirm the theoretical conclusion of the kinetic model that the SCPs of pure element shrink faster than alloyed particles. Wang et al. [88] considered in terms of molecular dynamic simulation the stability of CoPt single-crystalline nanoparticles of 10 nm in diameter and in the range of shell thicknesses of 0.5, 1.0 and 2.0 nm under the constant temperature of 300 K. It was indicated that the hollow nanoparticle with 0.5 nm shell thickness collapsed turning into solid one while the hollow nanoparticle with 1.0 nm shell thickness would shrink and finally stabilize as a smaller-sized hollow structure. The hollow nanoparticle with 2.0 nm shell thickness exhibited relatively higher stability against the shrinkage process. The influence of grain boundaries on the stability of polycrystal nanoparticles was analyzed by Valencia et al. [90]. It was shown that single-crystalline nanoparticles are more stable against the shrinkage process than their polycrystalline counterparts, which was attributed to the emission of partial dislocations from grain boundaries increasing the probability of partial void collapse. Valencia et al. [91] employed molecular dynamic simulation to investigate the thermal stability of porous hollow Au nanoparticles. It was demonstrated that shell porosity plays a major role in shrinkage process of porous hollow nanoparticles leading to a partial collapse of structure encouraged by lattice defects such as stacking faults and partial dislocations. Besides, the molecular dynamic simulation was employed to elucidate the cavity-formation process of Ag SCPs under ultrafast laser irradiation [93]. It was shown that no cavity formation was possible in the particle if the
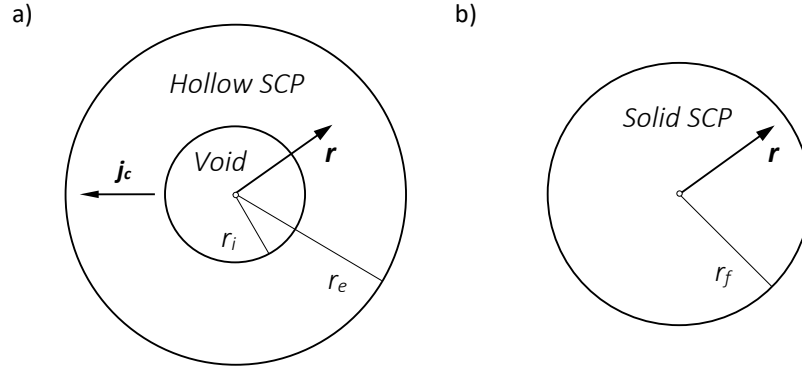
Fig. 3. Model of a SCP in its (a) initially hollow state with a central void and (b) final solid state after shrinking.

temperature was below 2000 K. In contrast, the hollow and porous hollow structures were observed under the temperature exceeded 3000 K.

2.1. Kinetic diffusion models

The void shrinkage kinetics in SCPs can be described analytically in terms of the bulk isotropic diffusion theory. According to this theory, the hollow SCPs are treated as isotropic homogeneous cylindrical or spherical shells of finite thickness with moving boundaries (Fig. 3). If a SCP is presumed to be defect-free, then the vacancy concentration C_v is governed by the following diffusion equations:

$$\Omega\, \mathbf{j}_c = -D_v \nabla C_v, \tag{1}$$

$$\frac{\partial C_v}{\partial t} = -\nabla \cdot (\Omega\, \mathbf{j}_c), \tag{2}$$

where $C_v = C_v(r,t)$ is the dimensionless concentration of vacancies, r is either the cylindrical or spherical radius-vector, t is the time, $\mathbf{j}_c$ is the vacancy flux density $[\mathrm{m}^{-2}\,\mathrm{s}^{-1}]$ corresponding to the concentration gradient between the internal $(r = r_i)$ and external $(r = r_e)$ surfaces, Ω is the atomic volume of a vacancy, D_v is the vacancy diffusion coefficient $[\mathrm{m}^2/\mathrm{s}]$, and ∇ is the Nabla operator.

Eqs. (1) and (2) can be rewritten as

$$\frac{1}{D_v}\frac{\partial C_v}{\partial t} = \Delta C_v, \tag{3}$$

where Δ is the Laplace operator. The initial condition for Eq. (3) is

$$C_v(r,t=0) = C_{v,0}(r). \tag{4}$$

For steady-state processes, the term $\partial C_v / \partial t$ is negligible and Eq. (3) transforms to

$$\Delta C_v = 0. \tag{5}$$

The Gibbs-Thompson curvature effect on the void evolution is described by the following boundary conditions:

$$C_v(r=r_i,t) = C_v^{eq}\exp\left(\frac{\beta}{r_i}\right), \tag{6a}$$

$$C_v(r=r_e,t) = C_v^{eq}\exp\left(-\frac{\beta}{r_e}\right), \tag{6b}$$

where C_v^{eq} is the equilibrium vacancy concentration in vicinity of a planar surface, β is a parameter: $\beta = 2\gamma\Omega / kT$ for a spherical particle and $\beta = \gamma\Omega / kT$ for a cylindrical particle; γ is the specific surface energy; k is the Boltzmann constant; T is the thermodynamic temperature. Eqs. (6a,b) allow to determine the concentration gradient between the particle surfaces, thus describing the vacancy migration from the inner surface to the outer one and the inverse migration of atoms from the outer surface to the inner one. The linear approximation of the Gibbs-Thompson conditions given by Eqs. (6a,b) gives

$$C_v^{eq}(r_i) \cong C_{v,0}\left(1+\frac{\beta}{r_i}\right), \tag{7a}$$

$$C_v^{eq}(r_e) \cong C_{v,0}\left(1-\frac{\beta}{r_e}\right). \tag{7b}$$

The motion of the particle surfaces due to the outward vacancy flux is defined as follows

$$\frac{dr_i}{dt} = -\frac{\Omega}{s_i}\oint \mathbf{n}\cdot\mathbf{j}_c\big|_{r=r_i}\, ds, \tag{8a}$$

$$\frac{dr_e}{dt} = -\frac{\Omega}{s_e}\oint \mathbf{n}\cdot\mathbf{j}_c\big|_{r=r_e}\, ds, \tag{8b}$$

where $\mathbf{n}$ is the outer normal to the particle surfaces, the surface parameters $s_{i,e} = 4\pi(r_{i,e})^2$ for a spherical particle and $s_{i,e} = 2\pi r_{i,e}$ for a cylindrical particle.

Finally, when the outward flow of vacancies is balanced by the inward flow of atoms, the volume of the particle material is assumed to remain unchanged during the shrinkage process, so that

$$V_e - \xi V_i = V_f,\qquad(9)$$

Where V_e and V_i are the volumes of the bodies bounded with the external and internal surfaces, respectively, V_f is the volume of the solid body, and the dimensionless parameter ξ reflects the effect of lattice relaxation in the first coordination spheres of atoms surrounding vacancies [94]. Fig. 4 demonstrates the dependence of the normalized particle radius r_e / r_f on the normalized void radius r_i / r_e for different values of ξ in the case of spherical particles. As is seen from Fig. 4, in the case of $\xi = 0.0$, the value of the solid particle radius r_f is underestimated due to the neglection of the outer radius change $(r_e = r_f)$, while for $\xi = 1.0$, the r_e value is overestimated due to the neglection of the lattice relaxation effect. One can also conclude that, for relatively small pores $(r_i / r_e < 0.5)$, the increase of particle size due to void evolution can be neglected ($\xi = 0.0$), while for relatively big pores $(r_i / r_e > 0.5)$, it is correct to use more accurate values $\xi \approx 0.5\ldots0.8$. In most theoretical calculations, the different contribution of vacancies and atoms in matter conservation law is neglected ($\xi = 1.0$).

Tu and Gösele [72] and Gusak et al. [84] were the first who considered the void stability problem in SCPs. In order to estimate the time needed to transform a hollow SCP to a solid one, the analytical solution of Eq. (5) under linear Gibbs-Thompson conditions given by Eqs. (7a,b) for the case of spherical geometry was found [72]:

$$C_v(r) = C_v^{eq}\beta\left(\frac{1}{\beta} - \frac{2}{r_e - r_i} + \frac{r_e + r_i}{r_e - r_i}\frac{1}{r}\right).\qquad(10)$$

Substituting Eq. (10) to Eq. (8a) gives the void surface evolution equation

$$\frac{dr_i}{dt} = \frac{D_v C_v^{eq}\beta}{r_i^2}\frac{r_e + r_i}{r_e - r_i}.\qquad(11)$$

The expected time of void collapse was determined from Eq. (11) for the two limiting cases of SCP geometry: (i) the case of a very thin shell $r_e \gg r_e - r_i$ and (ii) the case of a very thick shell $r_e \gg r_i$. The collapse time can be given for both the cases by formula:

$$t_f \cong \frac{kT}{A\gamma\Omega C_v^{eq}D_v}r_f^3,\qquad(12)$$

where r_f is the radius of a solid particle after the void collapse corresponding to the time t_f, A is a dimensionless parameter of the order of magnitude of ten.
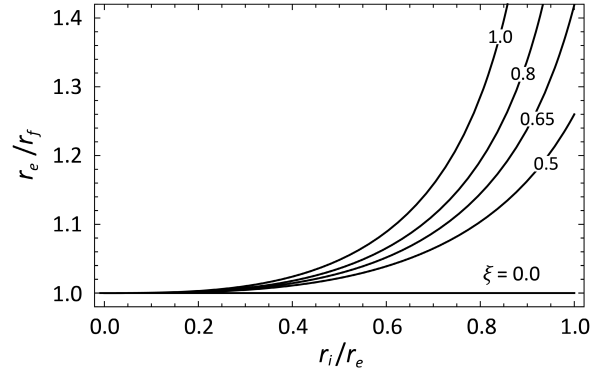
Fig. 4. Normalized relaxed radius r_e / r_f of a spherical particle with respect to the normalized void radius r_i / r_e for different values of $\xi = 0, 0.5, 0.65, 0.8,$ and 1.0.

For example, $A = 12$ for the case of a very thin shell [72] and $A = 6$ for the case of a very thick shell [84].

Evteev et al. [95] managed to obtain the following strict analytical solution of Eq. (11) for a shell of any finite thickness:

$$t_f = \frac{r_f^3}{6\beta D_v C_v^{eq}}\left[\frac{2\varepsilon}{\varepsilon^2 + \varepsilon + 1}\right.\\ \left.+\ln\frac{(\varepsilon^2 + \varepsilon + 1)(1 - \varepsilon^3)^{1/3}}{(\varepsilon + 1)^3}\right]\begin{array}{l}\varepsilon = r_i / r_e\\ \varepsilon = r_{i,0} / r_{e,0}\end{array},\qquad(13)$$

where $r_{i,0}$ and $r_{e,0}$ are the inner and outer particle radii at the initial moment of time $t = 0$. This solution demonstrates that the void collapse time depends not only on the final radius r_f of a solid particle, but also on the initial radii ratio of a hollow particle. Besides, the asymptotic behavior (expressions) for both the cases of very thin and very thick shell thicknesses were derived from Eq. (13).

The void evolution problem in SCPs was extended by Yanovsky et al. [96–98] to introduce the stability of eccentric voids filled with gas (so called bubbles). They considered the void evolution process as diffusion of both vacancies and gas atoms. The coupled problem concerning the classical diffusion theory in steady state approximation was set as

$$\Delta C_v = 0,\quad \Delta C_g = 0,\qquad(14)$$

where C_v and C_g are vacancy and gas concentration in the particle. These concentrations satisfy the boundary conditions on the internal and external particle surfaces:

$$C_v\Big|_{S_i} = C_v^{eq}\exp\left[\frac{\beta}{r_i} - \frac{P_i\Omega}{kT}\right],\qquad(15a)$$

$$C_v\Big|_{S_e} = C_v^{eq}\exp\left[-\frac{\beta}{r_e} - \frac{P_e\Omega}{kT}\right],\qquad(15b)$$
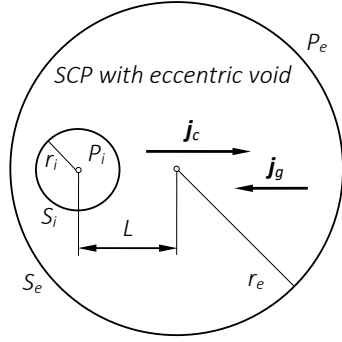
Fig. 5. Model of a SCP containing an eccentric gas-filled void.

$$C_g\Big|_{S_i} = P_i\kappa_H, \quad C_g\Big|_{S_e} = P_e\kappa_H, \tag{16a,b}$$

where P_i and P_e are the gas pressure inside and outside of hollow particle, S_i and S_e are the spherical void and particle surfaces, and κ_H is a coefficient which depends on whether gas atoms are of substitutional or interstitial type (see Fig. 5).

In this case, the void evolution kinetics is governed by the changes in the size and position of the void, and the gas density inside it:

$$\frac{dr_i}{dt} = -\frac{\Omega}{4\pi r_i^2}\oint \mathbf{n}\cdot\mathbf{j}_v\big|_{S_i} dS, \tag{17a}$$

$$\frac{dr_e}{dt} = -\frac{\Omega}{4\pi r_e^2}\oint \mathbf{n}\cdot\mathbf{j}_v\big|_{S_e} dS, \tag{17b}$$

$$\mathbf{v} = -\frac{3\Omega}{4\pi r_i^2}\oint \mathbf{n}\,\mathbf{n}\cdot\mathbf{j}_v\big|_{S_i} dS, \tag{18}$$

$$\frac{dN_g}{dt} = \oint \mathbf{n}\cdot\mathbf{j}_g\big|_{S_i} dS, \tag{19}$$

where $\mathbf{n}$ is the normal vector to a surface, N_g is the number of gas atoms inside the void, and $\mathbf{v}$ is the velocity of the void as a "rigid body" with respect to the particle.

The analytical solution of the boundary-value problem described by Eqs. (14,15) was found in a bi-spherical coordinate system that was the most convenient one for the case, in particular, to analyze numerically the void evolution equations given by Eqs. (11,12). Besides, the void collapse times for the limiting cases of very small and very large voids were derived asymptotically to verify the numerical results.

Yanovsky et al. [98] focused on the case when the external pressure is higher than the internal one, i.e., $P_e > P_i$. It was shown that the size and the position of the void are conserved until the gas pressure inside reaches the value of the external pressure. If the pressures inside and outside the particle are equalized, the void becomes unstable with respect to shrinkage and motion. In the special case of a symmetrically placed gas-filled void, the void evolution is determined by the shrinkage process only by the following set of equations

$$\frac{dr_i}{dt} = \frac{D_v}{r_i}\frac{(C_{v,e}-C_{v,i})r_e}{r_e-r_i}, \tag{20a}$$

$$\frac{dr_e}{dt} = \frac{D_v}{r_e}\frac{(C_{v,e}-C_{v,i})r_i}{r_e-r_i}, \tag{20b}$$

$$\frac{dN_g}{dt} = \frac{4\pi D_g}{\Omega}\frac{(C_{g,e}-C_{g,i})r_e r_i}{r_e-r_i}, \tag{21}$$

where D_g is the diffusivity of the gas atoms, $C_{v,i}$ and $C_{v,e}$ are the equilibrium vacancy concentrations on the internal and external surfaces, respectively, and $C_{g,i}$ and $C_{g,e}$ are the equilibrium concentrations of the gas atoms on the internal and external surfaces, respectively.

In contrast to the previous case, if the gas atom migration inside the particle is suppressed (i.e., the gas atom diffusivity is negligible, $D_g \to 0$), an optimal size of the void can be determined [97]. Since the gas atoms cannot migrate from the external surface to the internal one, the inner pressure is the only parameter to influence the void evolution. It was shown that the void tends to move to the particle center if the initial void size is bigger than the optimal one, while the void tends to move to the particle periphery if the initial void size is smaller than the optimal one.

In the limiting case of a symmetrical gas-filled void, assuming that the gas atom diffusivity is negligible, $D_g \to 0$, the evolution kinetic of the void is determined only by Eq. (20a). The equilibrium radius of the void can be determined from Eq. (20a) by using the condition $dr_i/dt = 0$ and the equation of ideal gas [97]:

$$r_{i,eq} = \frac{1}{2}\sqrt{\frac{3N_g kT}{2\pi\gamma}}. \tag{22}$$

The case of an eccentric vacancy void ($P_i = P_e = 0$) was studied by Yanovsky et al. [96]. It was noted that the void of any size and position are unstable and have a tendency to both shrinkage and rigid-body motion.

The main drawback of the aforementioned studies [96–98] is the fact that the void evolution process was considered without reference to the elastic stresses induced by the gas pressure inside the void. Besides, the authors did not analyze the equilibrium position of an arbitrary placed gas-filled void. However, these drawbacks do not depreciate the significance of the research.

The same phenomenon of void shrinkage occurs in polycrystalline particles (PCPs) of pure elements containing grain boundaries. In this case, the grain boundaries represent effective diffusion paths for vacancy flux (migration) from the particle center to the outer surface to accelerate shrinkage process. Klinger et al. [99] employed a weighed mean-curvature approach to derive the evolution equation of void shrinkage in PCPs with taking into consideration the grain-boundary diffusion (for two modes). Their results were illustrated by numerical dependencies of the void-to-particle volume ratio on time. The estimates show that the shrinkage process goes significantly faster in PCPs via grain-boundary diffusion than in SCPs via bulk diffusion. Besides, they predicted that hollow PCPs with certain number of grains above critical can be thermodynamically stable, in which case the internal void reaches an equilibrium size.

Kinetics models of void shrinkage in bi-alloyed particles were considered in Refs. [76,77,84,100].

The kinetic-diffusion approach was employed to investigate the void formation due to the Kirkendall effect in CShPs [102–105] and oxidated particles [101,106,107].

2.2. Models based on the thermodynamic extremal principle

The thermodynamic extremal principle (TEP) as a powerful tool for analyzing irreversible processes in materials science [99,108–110] was for the first time employed to study the void shrinkage kinetics in spherical SCPs by Fischer and Svoboda [111]. According to TEP, the Onsager principle of maximum can be employed to derive the void evolution equation by maximizing the system energy dissipation subjected to the constraint

$$Q = -\frac{dG}{dt}, \tag{23}$$

where Q is the total dissipation of energy in a process and G is the Gibbs total energy.

The energy dissipation due to the shrinkage process in hollow SCPs was considered to be caused by both the bulk diffusion and motion of inner and outer surfaces of SCPs:

$$Q = Q_B + Q_I, \tag{24a}$$

$$Q_B = \frac{4\pi R_g T}{\Omega D_v} \frac{r_i^2 (r_e - r_i)}{r_e} \left(\frac{dr_i}{dt}\right)^2, \tag{24b}$$

$$Q_I = 4\pi \left[r_i^2 \frac{1}{B_i} + \frac{r_i^4}{r_e^2} \frac{1}{B_e} \right] \left(\frac{dr_i}{dt}\right)^2, \tag{24c}$$

where R_g is the gas constant, B_i and B_e are the mobilities of the internal and external surfaces [111].

The total Gibbs energy of a hollow particles was determined as a sum

$$G = G_B + G_\tau + G_I, \tag{25a}$$

where

$$G_B = \frac{\pi E \varepsilon}{9(1-\nu)} \frac{(r_e - r_i)^4}{r_e^3 - r_i^3} \tag{25b}$$

is the contribution to the Gibbs energy due to the volumetric stress caused by inhomogeneous vacancy distribution inside the particle,

$$G_\tau = 4\pi \frac{\tau^2}{E}$$
$$\times \frac{[2(1-2\nu)(r_i^4 + r_e^4) + (1+\nu)(r_i^3 r_e + r_i r_e^3) + 6(1-\nu)r_i^2 r_e^2]}{r_e^3 - r_i^3} \tag{25c}$$

is the contribution to the Gibbs energy due to the stress state provoked by the surface tension on both the surfaces, and

$$G_I = 4\pi\gamma(r_i^2 + r_e^2) \tag{25d}$$

is the contribution to the Gibbs energy due to the presence of the internal and external surfaces. Here E is the Young modulus, ν is the Poisson coefficient, τ is the surface tension, and ε is the eigenstrain.

The evolution of a hollow particle can be derived from Eq. (23) according to the Onsager principle of maximum dissipation. To avoid too lengthy expressions, the authors of Ref. [111] used only the term $G = G_I$, thus considering the contributions of G_B and G_τ to be unimportant. Then, taking Eqs. (24) and (25d) into consideration, one can obtain the solution of Eq. (23) as

$$t = t_b + t_i + t_e = \int_{r_i}^{r_{i,0}} \frac{R_g T}{2\gamma\Omega D_v} \rho^2 \frac{R - \rho}{R + \rho} d\rho$$
$$+ \int_{r_i}^{r_{i,0}} \frac{\rho R}{2\gamma(R + \rho)B_i} d\rho + \int_{r_i}^{r_{i,0}} \frac{\rho^3}{2\gamma(R + \rho)RB_e} d\rho. \tag{26}$$

Considering both the surfaces as ideal vacancy sources and sinks, one can neglect the energy dissipation of surface motion to obtain the expression for collapse time analogous to the one found by Gusak et al. [84]:

$$t_{bf} \approx \frac{R_g T}{8\gamma\Omega D_v}\left(1-\frac{r_{i,0}}{r_{e,0}}\right)^3$$

$$\times\left[\frac{4}{3}-2\frac{r_{i,0}}{r_{e,0}}+\frac{8}{5}\left(\frac{r_{i,0}}{r_{e,0}}\right)^2+\frac{1}{15}\left(\frac{r_{i,0}}{r_{e,0}}\right)^3\right]. \qquad (27)$$

TEP was employed to investigate the void formation in metallic particles due to oxidation [112–114].

3. VOID FORMATION IN MULTIPLY TWINNED PARTICLES AS A CHANNEL OF RESIDUAL STRESS RELAXATION

3.1. The intrinsic structure of multiply twinned particles

The void evolution in face-centered cubic (FCC) crystalline multiply twinned particles (MTPs), which are a specific type of polyhedral crystalline particles (PCPs), is of special interest. The distinctive features of these particles are inhomogeneous residual stresses and strains induced by multiple cyclic twinning. As a result, MTPs often take shape of polyhedra with five-fold symmetry axes such as icosahedron, decahedron, pentagonal prism or plate [115–118] in spite of the fact that five-fold symmetry axes are forbidden in single crystals by the classical crystallography. In the case of decahedral particles (DhPs) and pentagonal whiskers (PWs) as the simplest representatives of MTPs, there is only one five-fold symmetry axis (see Fig. 6a,c), while icosahedral particles (IcPs) as more complicated representatives of MTPs, contain six such axes (Fig. 6e). These axes are the quintuple junctions of coherent twin boundaries of {111}-type and coincide with <011>-type crystallographic directions.

These quintuple junctions of twin boundaries induce inhomogeneous strains in MTPs, which have been properly experimentally investigated in the case of DhPs by electron microscopy [119–121]. The results of those researches confirm the disclination concept of inhomogeneous strain in MTPs [122,123], initially suggested independently by De Wit [124] and Galligan [125]. In accordance with this concept, a DhP can be constructed from five tetrahedral domains of a material with FCC crystalline structure, in which case the surface facets of the domains are the {111}-type crystallographic planes. These domains have to be glued together around an edge along <011>-type direction to form the decahedron (see Fig. 6b). This space-filling procedure is equivalent to introduction of a partial wedge disclination (WD) with strength

ω ~ 7.28° or 0.128 rd. Similar model treats PWs as pentagonal prisms elongated in <011>-type crystallographic direction and having {100}-type crystallographic planes on lateral prism facets and a WD of the same strength ω along the prism axis (Fig. 6d). The same procedure can be extended to IcPs containing six WDs of the same strength ω piercing the opposite vertexes of the icosahedron [122,126] (see Fig. 6e,f).

The continuum elastic models of MTPs are widely applied to describe the elastic inhomogeneous strain related to WDs. De Wit [124] was the first who suggested to use the stress and the strain energy of a straight positive WD of strength ω in a long cylinder for describing the strained state in PWs (see Fig 7a). Then a continuum elastic model of a DhP in the first approximation could be an elastic sphere with an axially symmetric positive WD of strength ω (Fig. 7b). Polonsky et al. [127] found for the first time an analytical solution for the elastic fields and energy of a WD in an elastic sphere. Kolesnikova et al. [128] extended this solution to the case of a WD in a hollow sphere. As was mentioned above, an IcP contains six positive WDs piercing the opposite vertices of the icosahedron. The elastic sphere containing six positive WDs could serve a continuum model of an IcP if the icosahedron shape would be replaced by the spherical one (Fig. 7c). However, Howie and Marks [129] suggested a much simpler model of stereo-disclination (SD called also Marks-Ioffe disclination) with strength χ ~ 0.0613 sr spread over the volume of the sphere (Fig. 7d).

According to these elastic models, the hydrostatic stress-tensor component of solid MTPs (PWs, IcPs, and DhPs) can be given in following forms:

$$^{cyl}\sigma_h^\omega = \frac{\mu\omega(1+\nu)}{3\pi(1-\nu)}\left(\frac{1}{2}+\ln\frac{r}{r_f}\right), \qquad (28)$$

$$^{sph}\sigma_h^\chi = \frac{4\mu\chi(1+\nu)}{3(1-\nu)}\left(\frac{1}{3}+\ln\frac{r}{r_f}\right), \qquad (29)$$

$$^{sph}\sigma_h^\omega = \frac{\mu\omega}{2\pi(1-\nu)}\left(2\ln(r\sin\theta)+\frac{1}{1-2\nu}\right)$$

$$-4\mu(1+\nu)\sum_{m=0}^{+\infty}\tilde{A}_m(2m+1)(4m+3)\left(\frac{r}{r_e}\right)^{2m}P_{2m}(\cos\theta), \qquad (30)$$

respectively, where μ is the shear modulus, θ is the polar angle in an appropriate spherical coordinate system (see Fig.7b), $P_n(x)$ is the Legendre polynomial, and $\tilde{A}_m$ is the series coefficient [128].

According to the aforementioned models, one can conclude that the central regions of MTPs are subjected to hydrostatic compression, while their
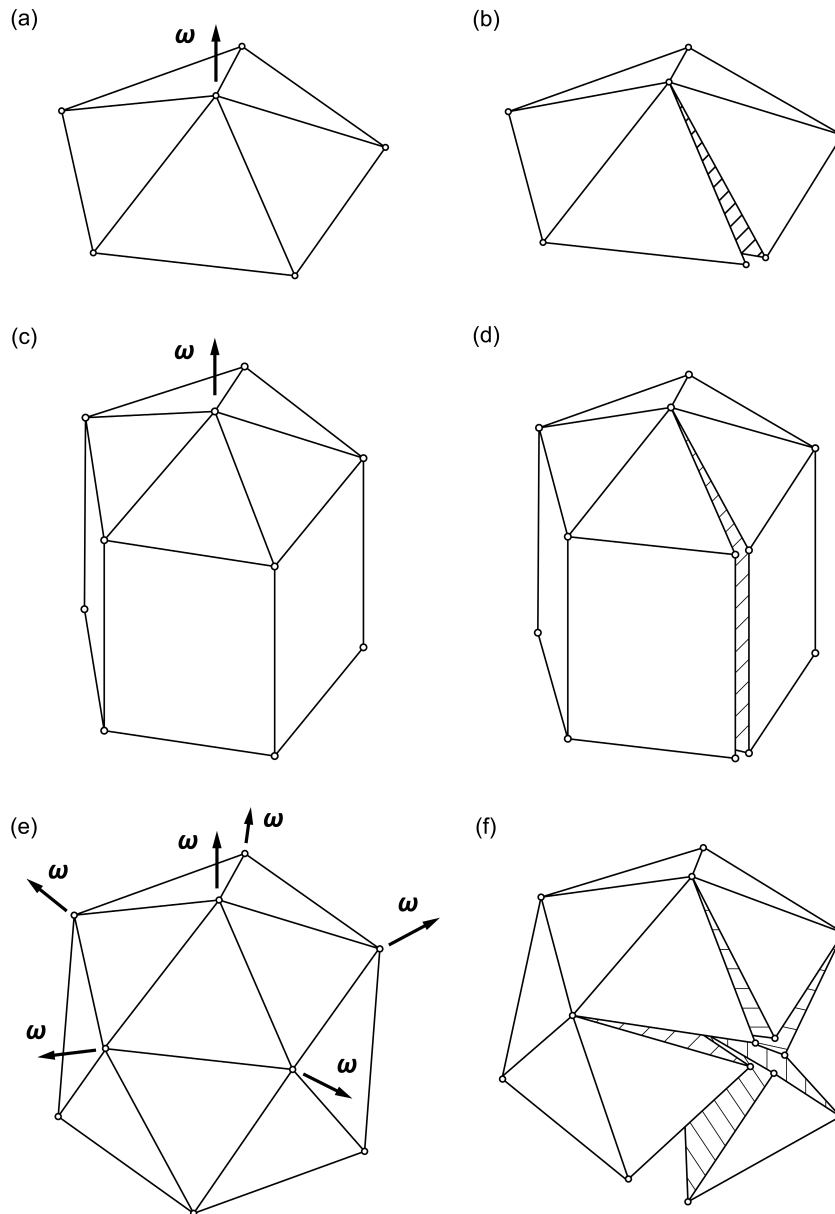
Fig. 6. Intrinsic structure of MTPs: (a,b) decahedral particles (DhP), (c,d) pentagonal whisker (PW) and (e,f) icosahedral particle (IcP). Figures (a,b,c) demonstrate elastically strained MTPs containing partial wedge disclinations (WDs) responsible for elimination of the gaps in model solid MTPs (b,d,f). Here ω is the Frank vector of a WD.

peripheral regions are subjected to tangential and hydrostatic tensions. Therefore, the stretched surfaces of MTPs can be considered as effective sources for vacancies that can further migrate to the central regions of MTPs. As a result, the inhomogeneous strain/stress state in MTPs can cause some supersaturation of vacancies in central regions of MTPs, which is induced by vacancy fluxes from the particle surfaces. Twin boundaries and WD cores serve as easy paths of vacancy diffusion. All these factors can provoke the spontaneous nucleation of voids. From the viewpoint of the energy balance, the void nucleation should decrease the stored strain energy and become an effective channel of residual stress

relaxation in MTPs. It is experimentally established that the inhomogeneous elastic strains and stresses, induced by five-fold cycling twinning, are responsible for formation of voids [130–134].

For instance, Huang et al. [134] investigated the influence of inhomogeneous strain on the void formation and growth in icosahedral bimetallic particles. They showed that heating of a mixture of solid strained icosahedral Pd particles in Cu solution can be employed to synthesize hollow Pd-Cu alloyed particles, while heating of a mixture of strain-free solid octahedral Pd particles in the Cu solution did not lead to void formation and, on the contrary, the solid Pd/Cu CShPs were produced. This means that the void occurrence
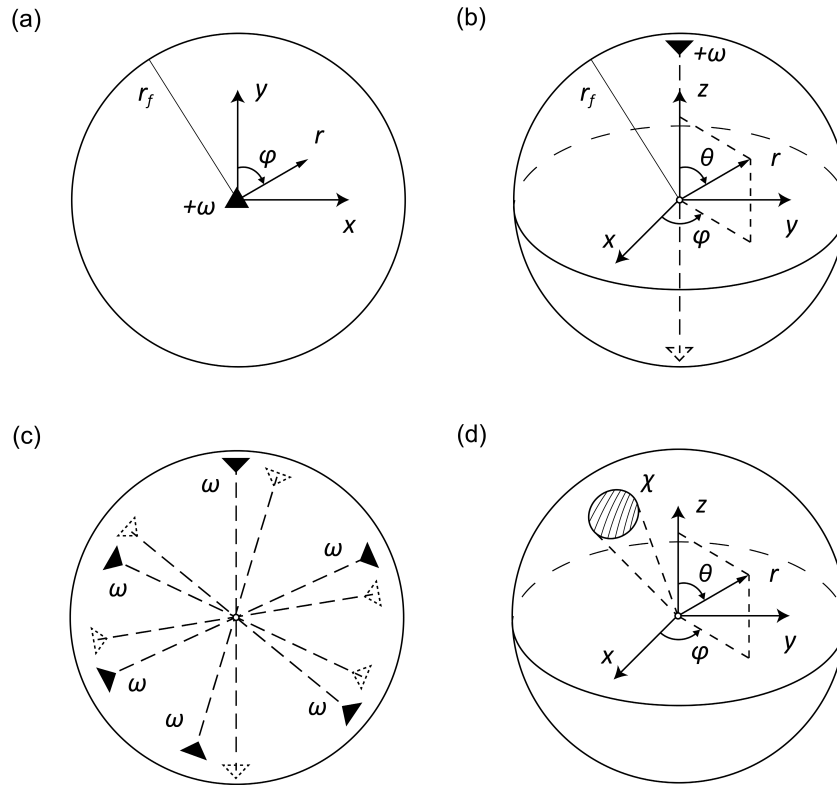
Fig. 7. The elastic models of MTPs: (a) a cross section of an elastic cylinder containing a positive WD of strength $\omega \approx 0.128$ as a continuum model of a PW; (b) an elastic sphere containing a positive WD of strength $\omega \approx 0.128$ as a continuum model of a DhP; (c) an elastic sphere containing six positive WDs, each of strength $\omega \approx 0.128$ as a continuum model of an IcP; (d) the Marks-Ioffe model of an IcP containing a stereo-disclination (SD) of strength $\chi \approx 0.0613$ sr.

in particles strongly depends on the inhomogeneous strain induced by multiply cycling twinning. In fact, the inhomogeneous strain is responsible for migration of the bigger atoms of Pd toward the peripheral stretched region of IcPs, while the smaller atoms of Cu and vacancies tend to migrate inward the central compressed region of IcPs. This imbalanced diffusion flux of matter stimulates the void formation process. In experiments, it was observed that the void nuclei initially occur at twin boundaries of IcPs with subsequent coalescence into a big central cavity. The authors of Ref. [134] applied the term "unexpected Kirkendall effect driven by strain gradient" to elucidate the void occurrence in bimetallic particles without considering the residual stress relaxation phenomenon. From our point of view, it would be more suitable to describe the void formation in IcPs as a channel of residual stress relaxion.

It is worth mentioning that hollows in MTPs can also be produced by different strategies using chemical etching [135] and surfactants [136], galvanic [137–139] and Kirkendall [140–142] replacement of components, and electron beam irradiation [143–145].

3.2. The quasi-equilibrium energy models of void formation in multiply twinned particles

The residual stress relaxation in MTPs can be investigated in terms of energy balance by quasi-equilibrium energy approach. According to this approach, MTPs are considered in terms of continuum disclination concept as elastic bodies containing WDs or SDs. The total energy of an initially defect-free MTP is compared with that one of a similar partly relaxed MTP containing structural defect(s). The formation of the defect(s) determines the stress relaxation channel. It is considered to be energetically favorable if the energy change between the MTP states, final and initial, is negative. This approach was employed to investigate the critical conditions of such different channels of stress relaxation in MTPs as: (i) the generation of circular prismatic dislocation loops in PWs [146], IcPs [147], DhPs [148] and core-shell nanoparticles with single-crystalline [149,150] and decahedral [151] structures; (ii) multiple cracks at twin boundaries of hollow DhPs and their subsequent agglomeration into a unite five-fold star crack [152]; (iii) formation of mismatched
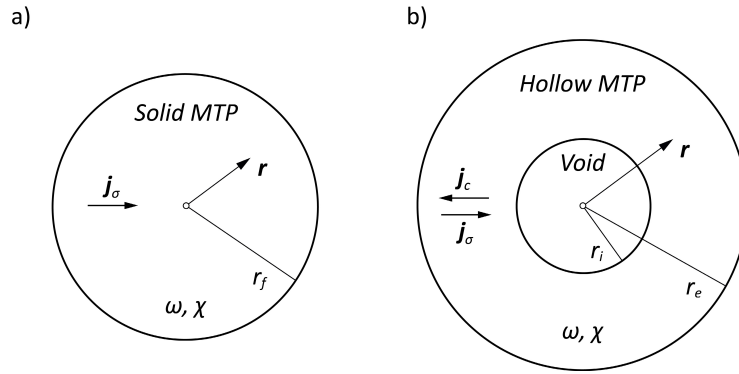
Fig. 8. Model of an MTP in its (a) initially solid state and (b) partially relaxed state with a central void.

layers in PWs [153,154] and IcPs [154,155]; and (iv) axial cylindrical misfitting inclusions in PWs [156,157]. Results of Refs. [149–152] are in agreement with experimental observation of misfit dislocations [158–160] and internal pores [132] in particles of different architectures.

The quasi-equilibrium energy approach was shown to be rather effective particularly in determining the critical conditions of void formation as a possible channel of stress relaxation in MTPs. Initially this relaxation channel was described theoretically for PWs and IcPs [130]. Recently, it has been extended to the case of DhPs [161] as well. In due course of these investigations, the following assumptions were employed: (i) an increase in the free surface area and the elastic strain relaxation were considered as the major factors responsible for the energy change; (ii) the energy contributions due to a decrease in the twin boundary area and some radial displacement of surface atoms caused by the surface tension were considered as negligible; (iii) the strain and surface energies of real (actual) MTPs were estimated as those of elastic bodies of either cylindrical or spherical geometry, containing the disclination defects.

According to the aforementioned works [130,161], initially solid MTPs under consideration can be treated as elastically isotropic cylinders (PWs) and spheres (IcPs and DhPs) of radius a_0, with shear modulus μ and Poisson ratio ν. Within such approach, the residual stresses in PWs and DhPs are described as those created by single axial positive partial WDs of strength $\omega \approx 0.128$ rd, whereas the residual stresses in IcPs are represented by those due to SDs of strength 0.0613 sr. As noted above, the central regions of MTPs are hydrostatically compressed while their peripheral regions are hydrostatically stretched (with the only exception of the small regions around the poles crossed by WDs in DhPs, which are compressed; see Fig. 8 in Ref. [128] for details). Such residual stress states can cause the generation of vacancies on the stretched surface of MTPs and

migration of vacancies to their central compressed regions with subsequent coagulation of the vacancies in a central void of radius r_i (see Fig. 8).

Generally, the total energy change of an MTP due to the void formation can be approximated by the following sum [130]:

$$\Delta E_{MTP} = \Delta E_{sf} + \Delta E_{tw} + \Delta E_{el} + \Delta E_{tn} + \Delta W_{el-sf}$$
$$+ \Delta W_{tn-sf} + \Delta W_{tn-el}, \tag{31}$$

where ΔE_{sf} is the free surface energy change, ΔE_{tw} is the twin boundary energy, ΔE_{el} is the disclination strain energy, ΔE_{tn} is the surface tension energy, ΔW_{el-sf} is the energy of interaction between the MTP free surface and the disclination stress field, ΔW_{tn-sf} is the energy of interaction between the MTP free surface and the elastic field caused by the surface tension, ΔW_{el-sf} is the energy of interaction between the elastic fields of the disclination and the surface tension. As was discussed above and demonstrated in [130], the contribution of twin boundaries and surface tension to the total energy change of MTPs can be neglected in comparison with the contribution of surface and strain energies. Therefore, Eq. (31) can be rewritten in the following simpler form

$$\Delta E = \Delta E_{sf} + \Delta E_{el}. \tag{32}$$

In Eq. (32), two main counteractive effects are considered: (i) an increase of the surface energy due to the formation of the new internal surface and (ii) a decrease of the disclination strain energy due to the residual stress relaxation. If the contribution of the latter one to the total energy change of an MTP is more significant, the void formation is considered to be energetically favorable. In other words, the stress relaxation through the void formation is energetically favorable if the corresponding total energy change of a MTP is negative, $\Delta E < 0$.

The surface energy ΔE_{sf} can be determined as

$$\Delta E_{sf} = \gamma (S_H - S_S), \tag{33}$$

where parameters S_H and S_S are introduced to describe the inner and outer surfaces of MTPs with regard to their polyhedral shapes. In the case of PWs,

$$S_H = \frac{5\sqrt{2}}{2}\sqrt{5-\sqrt{5}}\,(r_i + r_e), \tag{33a}$$

$$S_S = \frac{5\sqrt{2}}{2}\sqrt{5-\sqrt{5}}\,r_f, \tag{33b}$$

in the case of IcPs,

$$S_H = 2\sqrt{3}\left(5-\sqrt{5}\right)\left(r_i^2 + r_e^2\right), \tag{33c}$$

$$S_S = 2\sqrt{3}\left(5-\sqrt{5}\right)r_f^2, \tag{33d}$$

and in the case of DhPs,

$$S_H = \frac{5\sqrt{3}}{4}\left(5-\sqrt{5}\right)\left(r_i^2 + r_e^2\right), \tag{33e}$$

$$S_H = \frac{5\sqrt{3}}{4}\left(5-\sqrt{5}\right)r_f^2. \tag{33f}$$

The strain energy of a solid MTP can be approximated as the work spent on the creation of the corresponding disclination defect (either WD or SD) in its own stress field [127,130]:

$$^{cyl}E_{el}^{WD} = \frac{\mu\omega^2 r_f^2}{16\pi(1-\nu)}, \tag{34a}$$

$$^{sph}E_{el}^{SD} = \frac{8\pi}{27}\frac{1+\nu}{1-\nu}\mu\chi^2 r_f^3, \tag{34b}$$

$$^{sph}E_{el}^{WD} = \frac{\mu\omega^2 r_f^3}{2\pi(1-\nu)}\left[\frac{1}{6}\right.$$
$$\left. - \sum_{m=1}^{+\infty}\frac{(4m+3)(8\nu m^2 + 2m(5\nu^2+3\nu-1)+(1+\nu)(1+2\nu))}{2m(m+1)(2m+1)(2m+3)^2(4m^2+2m(1+2\nu)+1+\nu)}\right]. \tag{34c}$$

The strain energies of hollow MTPs [130,161] are

$$^{cyl}E_{el}^{WD} = \frac{\mu\omega^2 r_e^2}{16\pi(1-\nu)}\left(1 - \frac{r_i^2}{r_e^2} - \frac{9r_i^2}{r_e^2 - r_i^2}\ln^2\frac{r_i^2}{r_e^2}\right), \tag{35a}$$

$$^{sh}E_{el}^{SD} = \frac{8\pi}{27}\frac{1+\nu}{1-\nu}\mu\chi^2 r_e^3\left(1 - \frac{r_i^3}{r_e^3} - \frac{9r_i^3}{r_e^3 - r_i^3}\ln^2\frac{r_i}{r_e}\right), \tag{35b}$$

$$^{sh}E_{el}^{WD} = \frac{\mu\omega^2}{18\pi(1-\nu)}\left[(3\ln 2 - 1)(r_e^3 - r_i^3) - 3r_i^3\ln\frac{r_i}{r_e}\right.$$
$$\left. +(1+\nu)\left(\frac{5-6\ln 2}{3}(r_e^3 - r_i^3) + 2r_i^3\ln\frac{r_i}{r_e} - 3\frac{r_e^3 r_i^3}{r_e^3 - r_i^3}\ln^2\frac{r_i}{r_e}\right)\right]$$
$$-2\mu\omega\left[A_1\frac{7-4\nu}{5}(r_e^5 - r_i^5) + B_1\frac{r_e^3 - r_i^3}{3}\right.$$

$$+2C_1(1-2\nu)\ln\frac{r_i}{r_e} - D_1\frac{r_e^{-2} - r_i^{-2}}{2}$$
$$+\sum_{m=2}^{+\infty}\left(A_m(2m+5-4\nu)\frac{r_e^{2m+3} - r_i^{2m+3}}{2m+3} + B_m\frac{r_e^{2m+1} - r_i^{2m+1}}{2m+1}\right.$$
$$\left.\left. +C_m(m-2+2\nu)\frac{r_e^{-2m+2} - r_i^{-2m+2}}{m-1} - D_m\frac{r_e^{-2m} - r_i^{-2m}}{2m}\right)\right], \tag{35c}$$

where the expansion coefficients A_m, B_m, C_m and D_m can be found from the following set of algebraic equations issued from the boundary conditions on the inner ($r = r_i$) and outer surfaces ($r = r_e$) of the spherical shell [161]:

for $m = 0$,

$$\sigma_0(r = r_i)/(2\mu) - 2A_0(1+\nu) + D_0 r_i^{-3} = 0, \tag{36a}$$

$$\sigma_0(r = r_e)/(2\mu) - 2A_0(1+\nu) + D_0 r_e^{-3} = 0, \tag{36b}$$

with

$$\sigma_0 = -\frac{\mu\omega}{2\pi(1-\nu)}\frac{1+\nu}{9}\left(5 - 6\ln\frac{2r}{r_e}\right); \tag{37}$$

for $m \geq 1$,

$$\sigma_m(r = r_i)/(2\mu) + A_m(2m+1)(4m^2 - 2m - 2 - 2\nu)r_i^{2m}$$
$$+B_m 2m(2m-1)r_i^{2m-2} - C_m 2m(4m^2 + 6m - 2\nu)r_i^{-(2m+1)}$$
$$+D_m(2m+1)(2m+2)r_i^{-(2m+3)} = 0, \tag{38a}$$

$$\sigma_m(r = r_e)/(2\mu) + A_m(2m+1)(4m^2 - 2m - 2 - 2\nu)r_e^{2m}$$
$$+B_m 2m(2m-1)r_e^{2m-2} - C_m 2m(4m^2 + 6m - 2\nu)r_e^{-(2m+1)}$$
$$+D_m(2m+1)(2m+2)r_e^{-(2m+3)} = 0, \tag{38b}$$

$$\tau_m(r = r_i)/(2\mu) + A_m(2m+1)(4m^2 + 4m - 1 + 2\nu)r_i^{2m}$$
$$+B_m(2m-1)r_i^{2m-2} - C_m(4m^2 - 2 + 2\nu)r_i^{-(2m+1)}$$
$$-D_m(2m+2)r_i^{-(2m+3)} = 0, \tag{38c}$$

$$\tau_m(r = r_e)/(2\mu) + A_m(2m+1)(4m^2 + 4m - 1 + 2\nu)r_e^{2m}$$
$$+B_m(2m-1)r_e^{2m-2} - C_m(4m^2 - 2 + 2\nu)r_e^{-(2m+1)}$$
$$-D_m(2m+2)r_e^{-(2m+3)} = 0, \tag{38d}$$

with

$$\sigma_{m=1} = -\frac{\mu\omega}{2\pi(1-\nu)}\left(\frac{1-5\nu}{3} + \frac{1-2\nu}{45} - \frac{2(1-2\nu)}{3}\ln\frac{2r}{r_e}\right), \tag{39a}$$

$$\sigma_{m=2,3...} = \frac{\mu\omega}{2\pi(1-\nu)}\left(\frac{(1-2\nu)(2m-1)(m+1)(4m+1)}{(m-1)2m(2m+1)(2m+3)}\right.$$
$$\left. -\frac{4m+1}{2m(2m+1)}\right), \tag{39b}$$
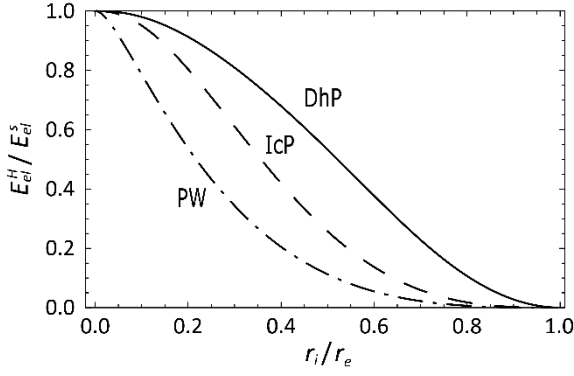
Fig. 9. The ratio of strain energies of hollow MTPs to solid ones in dependence on the inner-to-outer radii ratio r_i / r_e for DhP (solid curve), IcP (dashed curve) and PW (dash-dotted curve).

$$\tau_{m=1} = -\frac{\mu\omega}{2\pi(1-\nu)}\left(\frac{1-\nu}{3} + \frac{1-2\nu}{90} - \frac{1-2\nu}{3}\ln\frac{2r}{r_e}\right), \quad (39c)$$

$$\tau_{m=2,3...} = -\frac{\mu\omega}{2\pi(1-\nu)}\frac{(1-2\nu)(4m+1)}{(m-1)2m(2m+1)(2m+3)}. \quad (39d)$$

Fig. 9 shows the dependences of the ratio of the energy terms E_{el}^H and E_{el}^S given by Eqs. (34) and (35), respectively, on the inner to outer radii ratio r_i / r_e ($r_f = r_e$) for $\nu = 0.35$. As is seen, for all the cases under consideration (for DhPs, PWs, and IcPs), the strain energy decreases with an increase in the void radius. Moreover, at the same value of the inner to outer radii ratio, the strain energy ratio E_{el}^H / E_{el}^S takes the lowest value for PWs, a medium value for IcPs, and the highest value for DhPs. For example, at $r_i / r_e = 0.5$, these values are as follows: ~ 0.1 for PWs, ~ 0.25 for IcPs, and ~ 0.55 for DhPs. Thus, hollow DhPs store significantly higher strain energy than hollow PWs and IcPs of the same inner and outer radii.

Coming back to the surface and strain energy contributions in the relaxation process due to the void formation in MTPs, the corresponding energy change as a function of the initial radius r_f and the void radius r_e can be obtained

$$\Delta E_{MTP} = \gamma(S_H - S_S) + E_{el}^H - E_{el}^S. \quad (40)$$

We employ Eq. (40) to illustrate the energy change of MTPs under consideration as a function of the void radius r_i for different values of the initial radius r_f. In Fig. 10, the normalized curves of energy change $\Delta E_{MTP}(r_i / r_e)$ are demonstrated at $\nu = 0.3$ and $\gamma = Gb/8$ for (a) PWs, (b) IcPs, and (c) DhPs. In the framework of the quasi-equilibrium approach, the void formation in MTPs is energetically favorable if the corresponding energy change is negative, $\Delta E_{MTP} < 0$.
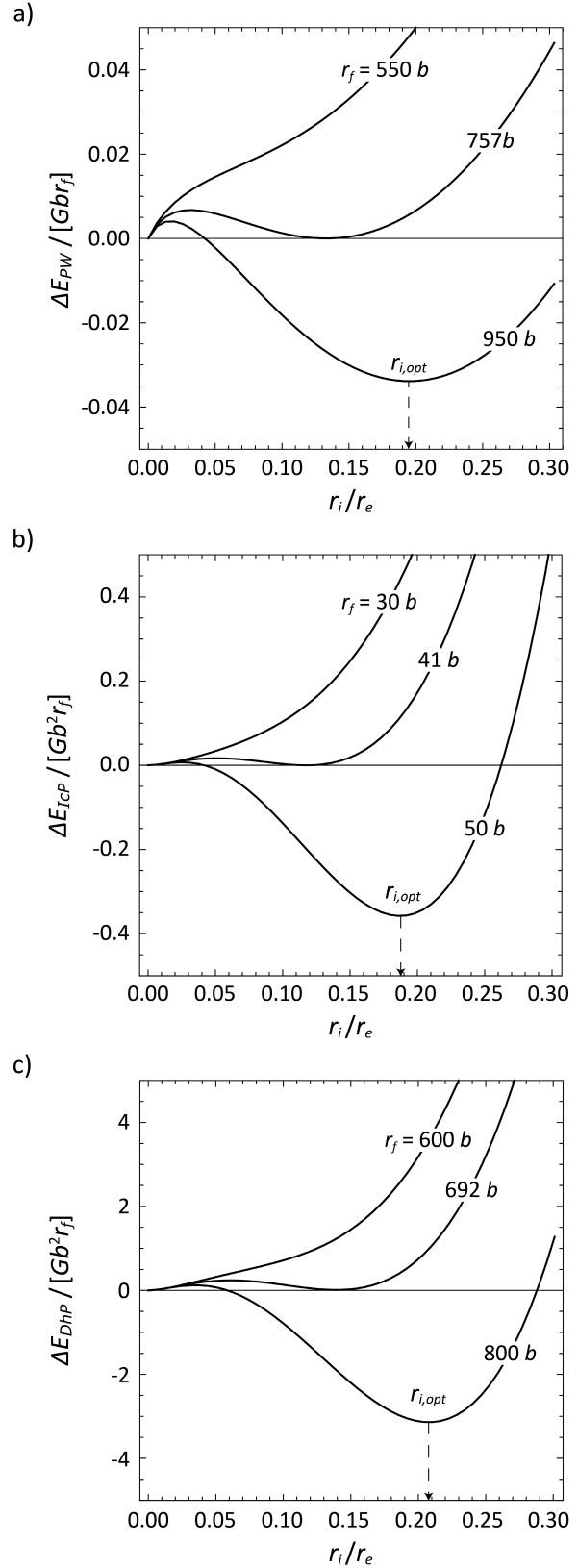
Fig. 10. The energy changes of different MTPs due to the void formation in dependence on the inner-to-outer radii ratio for different values of the initial radius r_f; (a) PW, (b) IcP, (c) DhP.

As is seen from Fig. 10, for all types of MTPs there exists a critical radius $r_{f,cr}$ of the initially solid structure so that the void formation is energetically unfavorable ($\Delta E > 0$ for any value of r_i) in MTPs of relatively small radius $r_f < r_{f,cr}$, while it is energetically favorable ($\Delta E < 0$ in a range of variable r_f) in MTPs of relatively large radius $r_f > r_{f,cr}$. This means that, in relatively small particles, the void is unstable and tends to shrinkage as it was observed in Au and Ag DhPs of 30–40 nm in diameter with voids of 3–8 nm in diameter [143–145]. The critical value of the MTP radius $r_{f,cr}$ can be determined numerically from the system of equations $\Delta E = 0$, $\partial \Delta E / \partial r_f = 0$, and $\partial^2 \Delta E / \partial r_f^2 > 0$. It is worth noting that the value of the critical radius $r_{f,cr} \sim 41b$ corresponding to IcPs is significantly less than the values $\sim 692b$ and $\sim 757b$ corresponding to critical radii of DhPs and PWs, respectively.

The critical radii of MTPs with regard to generation of circular prismatic dislocation loops were earlier calculated as $\sim 135b$ for PWs [146], $\sim 40b$ for IcPs [147] and $\sim 258b$ for DhPs [148] that is smaller than the results for pore formation (see Fig. 10b,c). One can conclude from this comparison that supersaturation of vacancies in center regions of IcPs induces either pore formation or the generation of vacancy-type prismatic dislocation loops while the vacancy supersaturation in PWs and DhPs could lead to generation of dislocation loop(s) of the same type with subsequent formation of a pore. The latter process has not been theoretically described yet.

In MTPs of radius $r_f > r_{i,cr}$, the void tends to grow up to an optimal radius $r_i = r_{i,opt}$ corresponding to the minimum of $\Delta E_{MTP} < 0$ (see Fig. 10). As is seen from Fig. 10, the more the initial radius r_f of the MTPs rises, the more the optimal normalized radius $r_{i,opt} / r_e$ of the pore is. Besides, Fig. 11 demonstrates how the optimal normalized radius $r_{i,opt} / r_e$ varies with the initial radius r_f of PWs, IcPs and DhPs in the case of pure Cu. It is seen that, for all MTPs under consideration, the curves gradually increase in the range of r_f from ~ 0.1 to ~ 2 μm with subsequent saturation. This result well agrees with experimental observation of large hollow DhPs and IcPs of radius $r_e > 0.5$ μm with thin shell thickness ~ 0.1 μm [132,133]. It is worth noting that the experimental values of $r_{i,opt} / r_e$ in DhPs were rather close to those in IcPs for relatively large values of r_e. Fig. 11 verifies theoretical results with the marks corresponding to experimental data on observation of hollow Cu MTPs attributed to stress relaxation processes. In fact, the theoretical curves are confirmed by the experimental points for all types of MTPs under consideration.
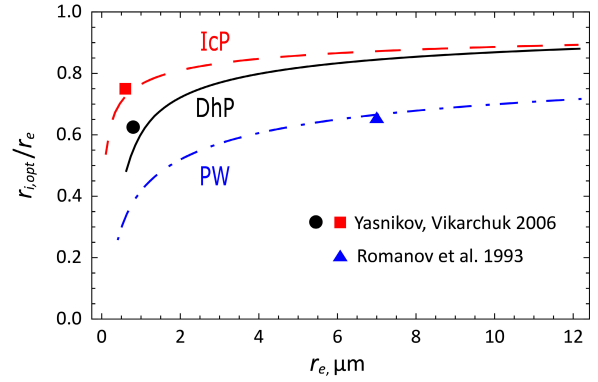
Fig. 11. Dependence of the normalized optimal radius of the pore $r_{i,opt} / r_e$ on the final radius r_e of different MTPs in pure Cu: DhP (black curve), IcP (red curve) and PW (blue curve). The experimental points (~ 0.8 μm, 0.63) and (~ 0.6 μm, 0.75) correspond to hollow DhPs and IcPs [132], respectively, while the experimental point (~ 7 μm, 0.66) corresponds to hollow PWs [130]. Adapted from Ref. [161].

3.3. The kinetic models of void formation in multiply twinned particles

The aforementioned quasi-equilibrium energy models are not effective enough to describe the void evolution kinetics in MTPs because the influence of the vacancy diffusion on this process was not taken into consideration. An attempt to overcome this limitation was taken by Vlasov et al. [162–164] who applied the bulk diffusion theory to investigate the initial-stage kinetics of phase transformation in MTPs via the migration of point defects (vacancies and impurity atoms) under the stress state induced by disclination defects. According to these works, the system of differential equations governing the concentration $C_v = C_v(r,t)$ of vacancies under strain gradient can be written as follows

$$\Omega\, \mathbf{j}_c + D_v \nabla C_v = 0, \tag{41a}$$

$$\Omega\, \mathbf{j}_\sigma + D_v \frac{C_v \nabla U}{kT} = 0, \tag{41b}$$

$$\frac{\partial C_v}{\partial t} + \Omega \nabla \cdot (\mathbf{j}_c + \mathbf{j}_\sigma) = 0, \tag{41c}$$

where r is either the cylindrical or spherical radius of a particle, $\mathbf{j}_c$ is the vacancy flux corresponding to the concentration gradient [see Eq. (1)], $\mathbf{j}_\sigma$ is the vacancy flux corresponding to the pressure gradient, Ω is the atomic volume, U is the potential of interaction between vacancies and the force (stress state) induced by vacancy sinks and sources such as dislocations, disclinations or grain boundaries, etc.

Substituting Eqs. (41a,b) to Eq. (41c), one can obtain the diffusion differential equation with a drift term:

$$\frac{1}{D_v}\frac{\partial C_v}{\partial t} = \Delta C_v + \frac{\nabla \cdot (C_v \nabla U)}{kT}. \tag{42}$$

Taking into consideration the Dirichlet boundary-value problem, the inner and outer particle surface is maintained (sustained, presumed) under the conditions of constant point defect concentration:

$$C_v(r = r_i, t) = C_p, \tag{43a}$$

$$C_v(r = r_e, t) = C_0, \tag{43b}$$

where C_p is the vacancy concentration at the void surface and C_0 is the average concentration of point defects.

Besides, the vacancy concentration should be defined at the initial moment of time:

$$C_v(r, t = 0) = C_0, \tag{44}$$

The evolution of the void surface is directly determined by vacancy migration driven by both the concentration gradient between particle surfaces and residual pressure in MTP:

$$\frac{dr_i}{dt} = -D_v \left[\mathbf{n} \cdot \nabla C_v + \frac{C_v}{kT} \mathbf{n} \cdot \nabla U \right]_{r=r_i}. \tag{45}$$

Eq. 45 gives the mass balance relation at void surface.

In the case of cylindrical geometry, Eq. (42) can be rewritten as

$$\frac{1}{D_v}\frac{\partial C_v}{\partial t} = \frac{\partial^2 C_v}{\partial r^2} + \frac{1+\alpha_2}{r}\frac{\partial C_v}{\partial r}, \tag{46a}$$

$$\alpha_2 = \frac{G\omega}{3\pi}\frac{1+\nu}{1-\nu}\frac{\delta v}{kT}, \tag{46b}$$

where δv is the change in the particle volume due to the formation of a vacancy, α_2 is the dimensionless parameter reflecting the contribution of the pressure-induced (drift) vacancy flux between the external and internal surfaces. When $|\alpha_2| \gg 1$, the drift flux prevails over the concentration-gradient flux and the contribution of the latter one can be assumed negligibly small. In contrast, when $|\alpha_2| \ll 1$, the distribution of vacancies is strongly governed by the concentration-gradient flux, while the contribution of the drift flux can be neglected. If $|\alpha_2| \approx 1$, the contributions of both the factors are comparable. In the case of PWs of pure Cu, the estimate of parameters gives $\alpha_2 \approx -1$. The sign of parameter α_2 is defined by the product of ω and δv. In this case, the relaxation volume of a vacancy is negative,

while the strength of the WD is positive. For $\alpha_2 = -1$, the solution of Eq. (46) reads

$$\frac{C_v - C_0}{C_p - C_0} = \frac{r_e - r}{r_e - r_i}$$
$$- \frac{2}{\pi}\sum_{n=1}^{+\infty}\frac{1}{n}\sin\left[\frac{\pi n(r-r_i)}{r_e - r_i}\right]\exp\left[-\frac{\pi^2 n^2 D_v t}{(r_e - r_i)^2}\right]. \tag{47}$$

The void growth rate is obtained from the mass balance equation (45) at the internal surface as follows

$$\frac{dr_i}{dt} = \frac{\Omega N_0 D_v(r_e C_p - r_i C_0)}{r_i(r_e - r_i)}$$
$$+ \frac{2\Omega N_0 D_v(C_p - C_0)}{r_e - r_i}\sum_{n=1}^{+\infty}\exp\left[-\frac{\pi^2 n^2 D_v t}{(r_e - r_i)^2}\right], \tag{48}$$

where N_0 is the number of atoms per unit volume.

In the steady state case ($\partial_t C_v \approx 0$), the void evolution is determined by the following equation:

$$\frac{dr_i}{dt} = \frac{\Omega N_0 D_v(r_e C_p - r_i C_0)}{r_i(r_e - r_i)}. \tag{49}$$

Presuming that $r_e C_p \gg r_i C_p$ and $\Omega N_0 \approx 1$, the integral of Eq. (49) gives a parabolic law for the void radius growth:

$$r_i = \sqrt{2C_p D_v t}. \tag{50}$$

Vlasov and Dragunov [163] extended the vacancy diffusion kinetics to the case of impurity atom migration to describe the new-phase growth in PWs. It is worth noting that the results obtained by kinetics models are applicable for both void and new phase growth. The Laplace-Carson integral transform was employed to derive Eq. (46) for two peculiar cases when (i) the contributions of concentration gradient and disclination stress are comparable; (ii) the contribution of concentration gradient is more significant than that one of disclination stress. The formal solutions of these equations are given by impurity atom concentrations represented in the Laplace-Carson space. Finally, the radius of a new (second) phase was derived from the transcendental equation obtained from the mass conservation condition on the interface under the assumption of parabolic nucleus growth.

Evolution equation (45) was employed by Vlasov and Zaznoba [164] to investigate the initial stage of the growth of a new phase nucleus in vicinity of structural defects including straight edge dislocations, crack tips, wedge and stereo disclinations. As the nucleus size at the initial stage is much less than the particle size, it was reasonable to use the pure drift flux assumption. It means that the concentration-gradient flux between the internal and external surfaces was considered

negligible, while the diffusion flux induced by defect pressure was assumed to play the main role. Under this assumption, the dependence of the internal radius of PWs and IcPs (described through WDs and SDs) on time was derived from Eq. (45) in the form of parabolic growth:

$$\frac{r_i}{b} = A_{1,2}\tau^{1/2}, \quad \tau = \frac{Dt}{b^2}, \quad A_{1,2} = \sqrt{2\alpha_{1,2}}, \qquad (51a,b)$$

where b is the interatomic distance in crystalline lattice, D is point defect diffusion, and the parameters $\alpha_{1,2}$ are defined as

$$\alpha_1 = \frac{G\chi}{3}\frac{1+\nu}{1-\nu}\frac{\delta v}{kT}, \quad \alpha_2 = \frac{G\omega}{3\pi}\frac{1+\nu}{1-\nu}\frac{\delta v}{kT}. \qquad (52a,b)$$

Hereinafter the subscript 1 refers to SDs, while the subscript 2 to WDs.

The number of vacancies absorbed by a SD is

$$N = B_1\tau^{3/2}, \quad B_1 = \frac{4\pi}{3}C_0\,\alpha_1^{3/2}, \qquad (53a)$$

and the number of vacancies per unit length absorbed by a WD is

$$N = B_2\tau, \quad B_2 = \frac{2\pi C_0\alpha_2}{b}, \qquad (53b)$$

where C_0 is the average concentration of the point defects.

Besides, the nucleus growth in vicinity of a straight edge dislocation and at a crack tip under external loading (without consideration of the angular dependence of

the hydrostatical stress) was investigated in Ref. [164] to provide a comparative analysis of nucleus kinetics in vicinity of various structural defects. In the case of interaction of point defects with the crack tip, the nucleus radius and the number of absorbed vacancies per unit length of the crack were found as functions of time:

$$\frac{r_i}{b} = A_3\tau^{2/5}, \quad A_3 = \left(\frac{5}{2}\frac{\alpha_3}{\sqrt{b}}\right)^{2/5}, \qquad (54a,b)$$

$$N = B_3\tau^{4/5}, \quad B_3 = \frac{\pi C_0}{b}\left(\frac{5}{2}\frac{\alpha_3}{\sqrt{b}}\right)^{4/5}, \qquad (54c,d)$$

$$\alpha_3 = \frac{(1+\nu)p_\infty}{3\sqrt{2}}\frac{\sqrt{a}\,\delta v}{kT}, \qquad (54e)$$

where p_∞ is the remote pressure and a is the half-length of the crack.

The nucleus radius and the number of vacancies segregated at a straight dislocation are determined by the following equations:

$$\frac{r_i}{b} = A_4\tau^{1/3}, \quad A_4 = \left(\frac{3\alpha_4}{b}\right)^{1/3}, \qquad (55a)$$

$$N = B_4\tau^{2/3}, \quad B_4 = \frac{\pi C_0}{b}\left(\frac{3\alpha_4}{b}\right)^{2/3}, \qquad (55c,d)$$

$$\alpha_4 = \frac{Gb}{3\pi}\frac{1+\nu}{1-\nu}\frac{\delta v}{kT}, \qquad (55e)$$

where b is the magnitude of the dislocation Burgers vector.
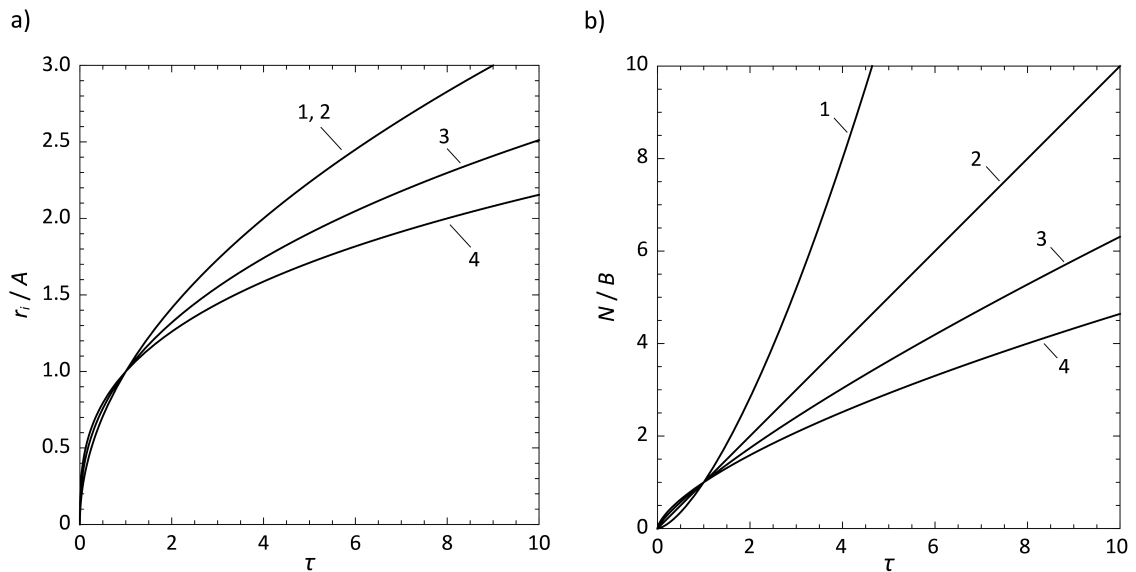
Fig. 12. The dependences of (a) the void radius and (b) the number of vacancies absorbed by different sinks (1 – SDs, 2 – WDs, 3 – crack tips, 4 – edge dislocations) on the normalized time τ. For simplicity, parameters A and B were assumed to be similar for all sinks under consideration.

The kinetics of nucleus growth at the initial stage in the vicinity of edge dislocations, crack tips, wedge and stereo disclinations, given by Eqs. (51)–(55), is shown in Fig. 12. As is seen from Fig. 12a, nuclei in MTPs (PWs and IcPs) grow faster in vicinity of SDs and WDs than in vicinity of crack tips and edge dislocations. Besides, SDs and WDs are the most essential sinks for point defect segregation, while crack tips and edge dislocations are less significant as shown in Fig. 12b illustrating the dependences of N on time τ for the defects under consideration.

Romanov and Samsonidze [165] investigated the diffusion of point defects in vicinity of a WD located in a cylinder with regard to generation of point defects at their sources and absorption of point defects at their sinks:

$$\frac{1}{\Omega}\frac{\partial C}{\partial t} = g - \nabla \cdot (\mathbf{j}_c + \mathbf{j}_\sigma) - D\kappa^2 C, \qquad (56)$$

where C is a concentration of the point defects, g is the rate of generation of point defects and κ^2 is the strength of their sink.

Besides, the boundary and initial conditions for concentration of point defects were considered with taking into account the stress field of the WD as follows

$$C(r = r_0, t) = C_{core} = C_{eq}\exp\left[-\frac{U}{kT}\right]_{r=r_0}$$
$$= C_{eq}\left(\frac{\sqrt{e}\,r_0}{r_e}\right)^{-\alpha_2}, \qquad (57a)$$

$$C(r = r_e, t) = C_{eq}\exp\left[-\frac{U}{kT}\right]_{r=r_e} = C_{eq}\left(\sqrt{e}\right)^{-\alpha_2}, \qquad (57b)$$

$$C(r, t=0) = C_{eq}\exp\left[-\frac{U}{kT}\right]_{t=0} = C_{eq}\left(\frac{\sqrt{e}\,r}{r_e}\right)^{-\alpha_2}, \qquad (57c)$$

where C_{eq} is the equilibrium concentration of point defects in a WD-free body and r_0 is the WD core radius.

The following expression for point defect flux at disclination core was obtained in Ref. [165]:

$$j(r = r_0, t) = \mathbf{e}_r \cdot \mathbf{j}|_{r=r_0} = \frac{D}{\Omega}\left\{\frac{\alpha_2 C_{core}}{r_0}\left[1 - \exp\left(-\kappa^2 Dt\right)\right]\right.$$
$$\left. + \left(\frac{g}{D\kappa^2} - C_{core}\right)\kappa\,\Phi\left(\kappa\sqrt{Dt}\right)\right\}, \qquad (58)$$

where C_{core} is determined by Eq. (57a) and $\Phi(x)$ is the error function. It is worth noting that Eq. (58) is applicable for describing either point defect diffusion at

initial stages where $t \sim r_0^2 / D$ or diffusion relating to quite strong point defect sinks where $t > 1/(\kappa^2 D)$. The first case is valid only if the point defects from vicinity of the core are absorbed by the WD, while the second one is valid if most point defects are absorbed by other sinks and only a small amount of point defect flux reaches the WD core.

A strict analytical solution of Eq. (56) was obtained under the assumption of steady state process. In Ref. [165], the expression of point defect flux is demonstrated without taking into account the presence of vacancy sinks ($\kappa^2 = 0$) as

$$j(r_0) = g r_0 \left| \frac{1}{2 + \alpha_2}\left[\frac{\alpha_2}{2}\frac{1 - r_e^2 / r_0^2}{(r_0^2 / r_e^2) - 1} - 1\right]\right|. \qquad (59)$$

The radius of voids nucleating in vicinity of the WD core was estimated under the assumption of steady state process in the following form

$$\frac{r_i}{r_0} \approx \left(1 + \frac{10^8 g r_0^2}{2\pi\rho}t\right)^{1/3}, \qquad (60)$$

where ρ is the linear void density $[m^{-1}]$.

The aforementioned models are restricted, however, by the limitation that the void kinetics cannot be thoroughly specified in terms of the new phase kinetics. In particular, the models by Vlasov et al. [162–164] do not give sufficient consideration to either the Gibbs-Thompson effect or the residual stress relaxation due to the void occurrence. More thorough investigation (analysis) of void kinetics in IcPs concerning both effects is presented in Ref. [166].

At the initial stages of void evolution in an IcP, the hydrostatic stress affecting the drift flux can be approximated by Eq. (29). This assumption seems to be quite appropriate for modeling the initial stages of the process if the void nucleus is much smaller than the IcP size. For final stages of the void growth, however, the following expression of the hydrostatic stress for a hollow IcP seems to be more applicable for theoretical analysis [166]:

$$^{sh}\sigma_h^\chi = \frac{4\mu\chi(1+\nu)}{3(1-\nu)}\left[\frac{1}{3} + \ln\frac{r}{r_e} - \frac{r_i^3}{r_e^3 - r_i^3}\ln\frac{r_e}{r_i}\right]. \qquad (61)$$

The gradient of the potential of interaction between vacancies and the hollow IcP is given by

$$\nabla U = -\delta v \nabla\left(^{sh}\sigma_h^\chi\right) = -\frac{4\delta v\mu\chi(1+\nu)}{3(1-\nu)}\frac{\mathbf{r}}{r^2}. \qquad (62)$$

Then the equation of the Fick second law for a spherical particle subjected to the SD stress fields in the steady-state process assumption reads

$$\Delta C_v - \frac{\alpha_1}{r^2}\left(r\frac{\partial C_v}{\partial r} + C_v\right) = 0, \tag{63}$$

where α_1 is defined by Eq. (52a).

A solution of the steady-state diffusion problem given by Eq. (63), satisfying the linear Gibbs-Thompson boundary conditions [see Eq. (7a)] on the inner and outer surfaces is

$$C_v(r) = C_v^{eq}\frac{(r_i+\beta)(r_e^{\alpha_1+1}-r^{\alpha_1+1})+(r_e-\beta)(r^{\alpha_1+1}-r_i^{\alpha_1+1})}{r(r_e^{\alpha_1+1}-r^{\alpha_1+1})}. \tag{64}$$

Notice that Eq. (64) for an IcP transforms to Eq. (10) for a SCP in the limiting case $\alpha_1 = 0$.

Fig. 13a shows the vacancy concentration profiles calculated numerically from Eq. (64) for different values of α_1. As is seen from Fig. 13a, in the cases of SCPs ($\alpha_1 = 0$) and IcPs ($\alpha_1 > 0$), the vacancy concentration at the inner and outer surfaces satisfies the Gibbs-Thompson conditions [see Eqs. (10)]. Besides, in the latter case, a local increase of vacancy concentration occurs in vicinity of the void surface — the less is the value of α_1 the higher is the concentration value and the closer the peak position to the void surface. In the limiting case of $\alpha_1 \to -\infty$, the vacancy flux is governed by the pressure gradient (the contribution of vacancy flux due to the surface Gibbs-Thompson effect is negligibly small), the peak of vacancy concentration reaches the void surface, and the concentration value takes a constant value $\sim 4.5\,C_{eq}$. The concentration profile for $\alpha_1 > 0$ could be interpreted as a result of diffusion of impurity atoms in IcPs. One can conclude that the concentration of impurities in hollow IcPs should be less than in SCPs. The minimum value of impurity concentration tends to move to the external surface with an increase in α_1. In the limiting case of $\alpha_1 \to +\infty$, the impurity concentration takes a constant value $\sim 0.3\,C_{eq}$ at the outer surface of the hollow IcP.

The void evolution can be determined by the mass balance equation at the void surface [see Eq. (45)]. Substituting Eq. (64) to Eq. (45), one can obtain the following void evolution equation in an IcP:

$$\frac{d\varepsilon}{d\tau} = \frac{(\alpha_1+1)[(1-\varepsilon^3)^2(\varepsilon^{\alpha_1+1}+1)-(\beta/r_f)\varepsilon(1-\varepsilon^3)^{5/3}(\varepsilon^{\alpha_1}-1)]}{6\varepsilon^2(\varepsilon^{\alpha_1+1}-1)}, \tag{65}$$

where the following denotations and equations are used:

$$\varepsilon = \frac{r_i}{r_e}, \quad r_i = \frac{\varepsilon r_f}{(1-\varepsilon^3)^{1/3}}, \quad r_e = \frac{r_f}{(1-\varepsilon^3)^{1/3}},$$

$$\tau = \frac{6D_v C_v^{eq} t}{r_f^3}. \tag{66a–d}$$

a)

b)
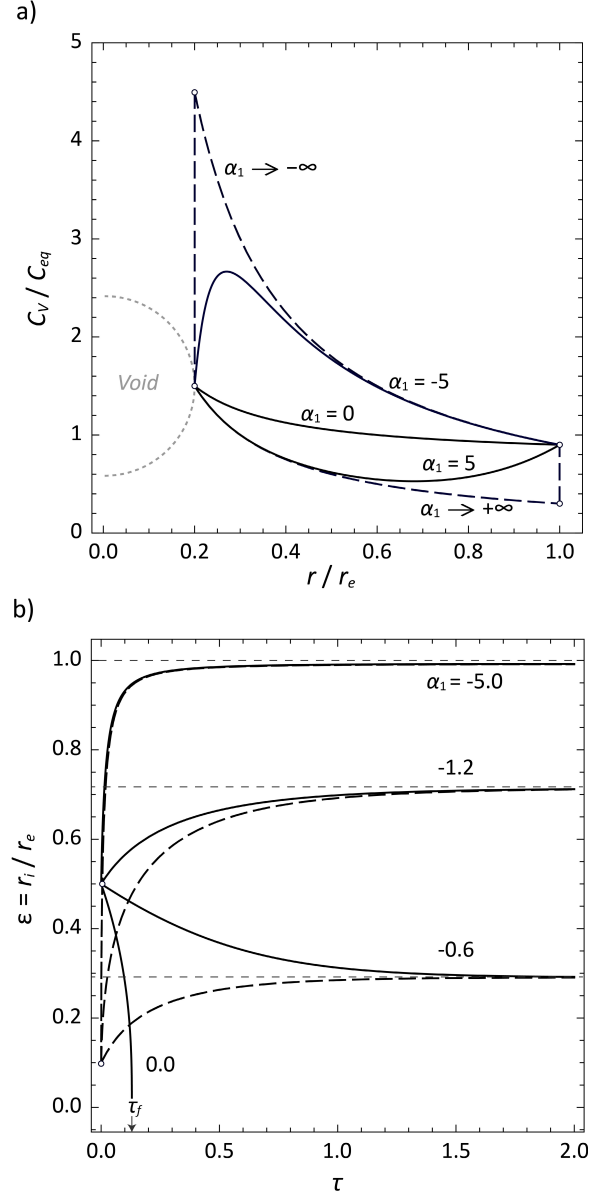
Fig. 13. (a) The vacancy concentration profiles C_v / C_{eq} with respect to the normalized distance r/r_e from the center of the hollow IcPs for different values of α_1 at $r_i/r_e = 0.2$ and $\beta/r_e = 1/3$. The dashed curves correspond to the limiting cases of $\alpha_1 \to \pm\infty$. (b) The dependence of the normalized void radius $\varepsilon = r_i/r_e$ on the normalized time τ at $\beta/r_f = 1/5$ for different values of $\alpha_1 = -0.6, -1.2, -5$ and the initial void radii $r_{i,0} = 0.5 r_e$ (the solid curves) and $0.1 r_e$ (the dashed curves).

The solution of Eq. (65) was obtained by numerical integration and illustrated in Fig. 13b. The curves $\varepsilon(\tau)$ are shown for different values of α_1 and initial normalized void radius $\varepsilon_0 = r_{i,0}/r_{e,0}$. As is seen from Fig. 13b, the scenario of void evolution in IcPs strongly depends on the initial void radius and the value of α_1. In the case of $\alpha_1 = 0$, for any values of ε_0, the void tends to

shrinkage and finally collapses at the time $\tau = \tau_f$ as it was shown by Evteev et al. [95]. For $\alpha_1 = -0.6$, the void tends to reach some equilibrium size $\varepsilon_{eq} = r_{i,eq} / r_e$ via growing (when $\varepsilon_0 < \varepsilon_{eq}$) or shrinking (when $\varepsilon_0 > \varepsilon_{eq}$). It is worth noting that, for relatively small values of $\alpha_1 < -1$, solid IcPs could be transformed into thin spherical shells (see, for example, the curve for $\alpha_1 = -5$).

Tsagrakis et al. [167] made an attempt to describe the void evolution kinetics in IcPs in terms of the strain-gradient elasticity. The gradient elastic model of an IcP was suggested to obtain the hydrostatic stress induced by a SD (Marks-Ioffe disclination). The hydrostatic stress was given by

$$^{sph}\sigma_h^{\chi,\lambda} = \frac{4\mu\chi(1+\nu)}{3(1-\nu)}\left\{\frac{1}{3}+\ln\frac{r}{r_e}-\frac{\lambda}{r}\cosh\left(\frac{r}{\lambda}\right)\mathrm{Shi}\left(\frac{r}{\lambda}\right)\right.$$
$$\left.-\frac{\lambda}{r}\sinh\left(\frac{r}{\lambda}\right)\left[C_1+\mathrm{Chi}\left(\frac{r}{\lambda}\right)\right]\right\}, \quad (67a)$$

$$C_1 = \frac{\lambda}{r_e\hat{I}_{3/2}(r_e/\lambda)}\left[1+\frac{r_e}{\lambda}\mathrm{Shi}\left(\frac{r_e}{\lambda}\right)\hat{I}_{-3/2}\left(\frac{r_e}{\lambda}\right)\right]-\mathrm{Chi}\left(\frac{r_e}{\lambda}\right),$$
$$(67b)$$

where λ is some intristic length corresponding to non-local gradient effects, Shi(x) and Chi(x) are hyperbolic sine and cosine integrals, respectively, $\hat{I}_{n/2}(x) = \sqrt{\pi/2x}I_{n/2}(x)$, $I_{n/2}(x)$ is the modified Bessel function [167]. Fig. 14a shows the dependences of hydrostatic stress on the normalized distance from the IcP center for different values of λ. The gradient solution given by Eq. (67) is advantageous as it takes regular values at the IcP center, in contrast to the classical solution given by Eq. (29).

In Ref. [167], a stress-assisted diffusion model was employed to approximate the point defect flux as follows:

$$\Omega\,\mathbf{j} = -(D + N\,^{sph}\sigma_h^{\chi,\lambda})\nabla C + M\,C\nabla\left(^{sph}\sigma_h^{\chi,\lambda}\right), \quad (68)$$

where C is the concentration of point defects, D is their diffusivity, M and N are some extra diffusion constants. The diffusion equation can be obtained by substituting Eq. (68) in continuity equation that results in

$$\frac{\partial C}{\partial t} = (D + N\,^{sph}\sigma_h^{\chi,\lambda})\Delta C - (M - N)\nabla\left(^{sph}\sigma_h^{\chi,\lambda}\right)\cdot\nabla C$$
$$-M\,C\,\Delta\left(^{sph}\sigma_h^{\chi,\lambda}\right). \quad (69)$$

The steady state solution of Eq. (69) reads:

$$C(r) = 1 - (1 - C_e)\left[\frac{1 + B\,^{sph}\sigma_h^{\chi,\lambda}(r)}{1 + B\,^{sph}\sigma_h^{\chi,\lambda}(r_e)}\right]^A, \quad (70)$$

a)

b)
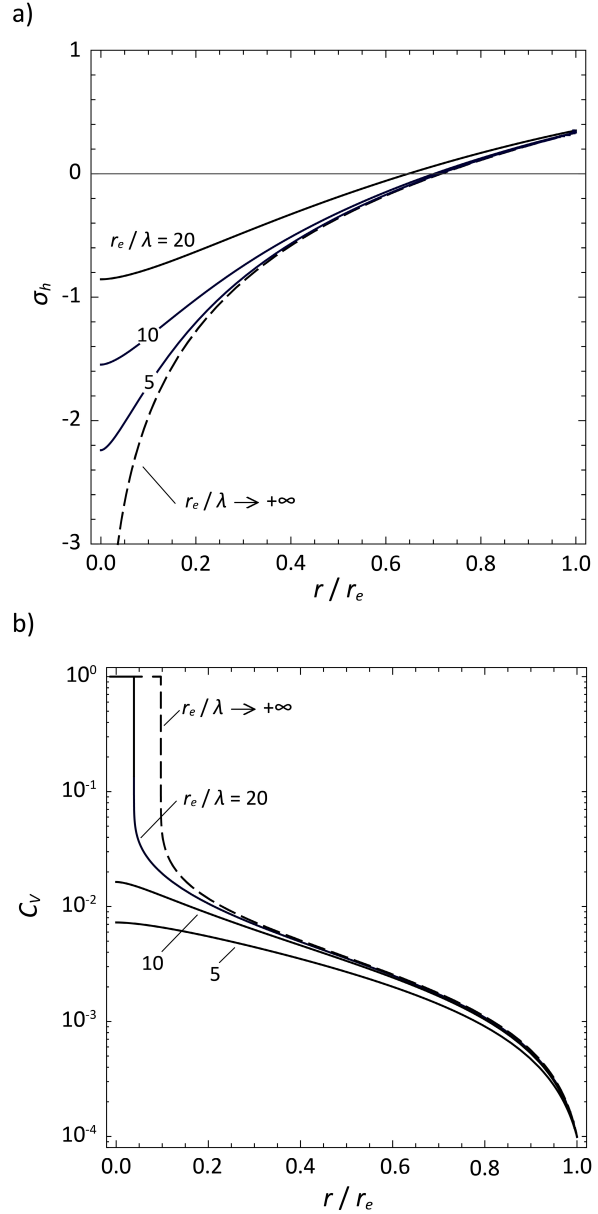
Fig. 14. The dependences of (a) the hydrostatic stress and (b) the relative vacancy concentration on the normalized distance r/r_e from the center of an IcP with respect to the classical elasticity (dashed curves) and the strain-gradient elasticity (solid curves) for different values of the parameter $r_e/\lambda = 5, 10, 20$. The hydrostatic stress is given in units of $4\mu(1+\nu)/[3(1-\nu)]$. The concentration profiles in (b) are illustrated for prescribed vacancy concentration at the external IcP surface $C_e = 10^{-4}$ at $A = 10^{-2}$ and $B = 1/2$. Adapted from Ref. [167].

where C_e is the vacancy concentration at the external surface of the IcP, $A = M/N$ and $B = N/D$.

Eq. (69) gives the vacancy redistribution in an IcP with taking into consideration the gradient solution for the residual stress state. Fig. 14b shows the

concentration profiles determined by Eq. (69) for different values of λ.

4. CONCLUSIONS

This review is focused on various theoretical approaches and methods employed to describe the void evolution in micro/nanoparticles of pure chemical elements. The first part of the review contains a brief description of hollow structures including their classification, various aspects of their application, different strategies of void synthesis and the discussion of the main factors governing the void evolution phenomena. The second part presents a complete description of analytical models of void evolution in SCPs classified with regard to the main principles of diffusion kinetics and equilibrium thermodynamics. In particular, the analysis of void stability in SCPs with respect to shrinking was properly discussed. The third part of the review is devoted to void generation in MTPs as a channel of residual stress relaxation. Models of void growth are sorted out in accordance with the quasi-equilibrium energy approach and the diffusion kinetic theory. The evolution of void structures in inhomogeneous particles (such as MTPs and CShPs) is deemed to be highly potential issue for further thorough investigation in terms of mutual analysis of Gibbs-Thomson and Kirkendall effects and residual stress impact.

REFERENCES

[1] I. Hussain, S. Sahoo, M.S. Sayed, M. Ahmad, M.S. Javed, C. Lamiel, Yu. Li, J.-J. Shim, X. Ma and K. Zhang, *Hollow nano-and microstructures: Mechanism, composition, applications, and factors affecting morphology and performance*, Coordination Chemistry Reviews, 2022, vol. 458, art. no. 214429. https://doi.org/10.1016/j.ccr.2022.214429

[2] M. Zhao, X. Wang, X. Yang, K.D. Gilroy, D. Qin and Y. Xia, *Hollow metal nanocrystals with ultrathin, porous walls and well-controlled surface structures*, Advanced Materials, 2018, vol. 30, no. 48, art. no. 1801956. https://doi.org/10.1002/adma.201801956

[3] M. Guarino-Hotz and J.Z. Zhang, *Structural control and biomedical applications of plasmonic hollow gold nanospheres: A mini review*, Wiley Interdisciplinary Reviews: Nanomedicine and Nanobiotechnology, 2021, vol. 13, no. 4, art. no. e1694. https://doi.org/10.1002/wnan.1694

[4] J. Richard-Daniel and D. Boudreau, *Enhancing galvanic replacement in plasmonic hollow nanoparticles: Understanding the role of the speciation of metal ion precursors*, ChemNanoMat, 2020, vol. 6, no. 6, pp. 907–915. https://doi.org/10.1002/cnma.202000158

[5] A. Genç, J. Patarroyo, J. Sancho-Parramon, N.G. Bastús, V. Puntes and J. Arbiol, *Hollow metal nanostructures for enhanced plasmonics: synthesis, local plasmonic properties and applications*, Nanophotonics, 2017, vol. 6, no. 1, pp. 193–213. https://doi.org/10.1515/nanoph-2016-0124

[6] Y.Z. Wang, M. Yang, Y.-M. Ding, N.-W. Li and L. Yu, *Recent advances in complex hollow electrocatalysts for water splitting*, Advanced Functional Materials, 2022, vol. 32, no. 6, art. no. 2108681. https://doi.org/10.1002/adfm.202108681

[7] Z. Li, M. Song, W. Zhu, W. Zhuang, X. Du and L. Tian, *MOF-derived hollow heterostructures for advanced electrocatalysis*, Coordination Chemistry Reviews, 2021, vol. 439, art. no. 213946. https://doi.org/10.1016/j.ccr.2021.213946

[8] J. Park, T. Kwon, J. Kim, H. Jin, H.Y. Kim, B. Kim, S. H. Joo and K. Lee, *Hollow nanoparticles as emerging electrocatalysts for renewable energy conversion reactions*, Chemical Society Reviews, 2018, vol. 47, no. 22, pp. 8173–8202. https://doi.org/10.1039/C8CS00336J

[9] T. Asset, R. Chattot, M. Fontana, B. Mercier-Guyon, N. Job, L. Dubau and F. Maillard, *A review on recent developments and prospects for the oxygen reduction reaction on hollow Pt-alloy nanoparticles*, ChemPhysChem, 2018, vol. 19, no. 13, pp. 1552–1567. https://doi.org/10.1002/cphc.201800153

[10] S.H. Raad and Z. Atlasbaf, *Solar cell design using graphene-based hollow nano-pillars*, Scientific Reports, 2021, vol. 11, art. no. 16169. https://doi.org/10.1038/s41598-021-95684-2

[11] M. Xiao, Z. Wang, M. Lyu, B. Luo, S. Wang, G. Liu., H.-M. Cheng and L. Wang, *Hollow nanostructures for photocatalysis: advantages and challenges*, Advanced Materials, 2019, vol. 31, no. 38, art. no. 1801369. https://doi.org/10.1002/adma.201801369

[12] W. Hu, M. Zheng, B. Xu, Y. Wei, W. Zhu, Q. Li, and H. Pang, *Design of hollow carbon-based materials derived from metal-organic frameworks for electrocatalysis and electrochemical energy storage*, Journal of Materials Chemistry A, 2021, vol. 9, no. 7, pp. 3880–3917. https://doi.org/10.1039/D0TA10666F

[13] X.-Y. Yu, L. Yu and X.W. Lou, *Metal sulfide hollow nanostructures for electrochemical*

energy storage, Advanced Energy Materials, 2016, vol. 6, no. 3, art. no. 1501333. https://doi.org/10.1002/aenm.201501333

[14] L. Yu, H. Hu, H.B. Wu and X.W. Lou, *Complex hollow nanostructures: synthesis and energy-related applications*, Advanced Materials, 2017, vol. 29, no. 15, art. no. 1604563. https://doi.org/10.1002/adma.201604563

[15] J. Wang, Y. Cui and D. Wang, *Design of hollow nanostructures for energy storage, conversion and production*, Advanced Materials, 2019, vol. 31, no. 38, art. no. 1801993. https://doi.org/10.1002/adma.201801993

[16] B.B. Galabova, *Mesoporous silica nanoparticles: Synthesis, functionalization, drug loading and release – A review*, Tropical Journal of Pharmaceutical Research, 2021, vol. 20, no. 5, pp. 1091–1100. http://doi.org/10.4314/tjpr.v20i5.30

[17] D. Jiang, Q. Zhang, C. Xu, Y. Ge, L. Huang, X. Ren and Y. Wang, *Facile preparation of a hollow core-shell nanocomposite for the ultrasensitive sensing of glucose*, Sensors and Actuators B: Chemical, 2020, vol. 321, art. no. 128500. https://doi.org/10.1016/j.snb.2020.128500

[18] K. An and T. Hyeon, *Synthesis and biomedical applications of hollow nanostructures*, Nano Today, 2009, vol. 4, no. 4, pp. 359–373. https://doi.org/10.1016/j.nantod.2009.06.013

[19] B.K. Juluri, J. Huang and L. Jensen, *Extinction, scattering and absorption efficiencies of single and multilayer nanoparticles*, 2010, https://nanohub.org/resources/8228

[20] J.-H. Lee, *Gas sensors using hierarchical and hollow oxide nanostructures: overview*, Sensors and Actuators B: Chemical, 2009, vol. 140, no. 1, pp. 319–336. https://doi.org/10.1016/j.snb.2009.04.026

[21] T. Wang, X. Kou, L. Zhao, P. Sun, C. Liu , Y. Wang, K. Shimanoe, N. Yamazoe and G. Lu, *Flower-like ZnO hollow microspheres loaded with CdO nanoparticles as high performance sensing material for gas sensors*, Sensors and Actuators B: Chemical, 2017, vol. 250, pp. 692–702. https://doi.org/10.1016/j.snb.2017.04.099

[22] X. Wang, F. Liu, X. Chen, G. Lu, X. Song, J. Tian, H. Cui, G. Zhang and K. Gao, *SnO$_2$ core-shell hollow microspheres co-modification with Au and NiO nanoparticles for acetone gas sensing*, Powder Technology, 2020, vol. 364, pp. 159–166. https://doi.org/10.1016/j.powtec.2020.02.006

[23] Z. Liu, Z. Yang, B. Peng, C. Cao, C. Zhang, H. You, Q. Xiong, Z. Li and J. Fang, *Highly sensitive, uniform, and reproducible surface-enhanced Raman spectroscopy from hollow Au-Ag alloy nanourchins*, Advanced Materials, 2014, vol. 26, no. 15, pp. 2431–2439. https://doi.org/10.1002/adma.201305106

[24] S. Jeong, M.-W. Kim, Y.-R. Jo, N.-Y. Kim, D. Kang, S.Y. Lee, S.-Y. Yim, B.-J. Kim and J.H. Kim, *Hollow porous gold nanoshells with controlled nanojunctions for highly tunable plasmon resonances and intense field enhancements for surface-enhanced Raman scattering*, ACS Applied Materials and Interfaces, 2019, vol. 11, no. 47, pp. 44458–44465. https://doi.org/10.1021/acsami.9b16983

[25] Y. Zhang, H. Wu, Z. Liu, S. Xie and J. Li, *Hollow spheres self-assembled by MoO$_2$ nanocones as highly sensitive substrate for Surface-Enhanced Raman Spectroscopy*, Journal of Materiomics, 2021, vol. 7, no. 2, pp. 347–354. https://doi.org/10.1016/j.jmat.2020.06.008

[26] M.S. Zielinski, J.-W. Choi, T. La Grange, M. Modestino, S.M.H. Hashemi, Y. Pu, S. Birkhold, J.A. Hubbell and D. Psaltis, *Hollow mesoporous plasmonic nanoshells for enhanced solar vapor generation*, Nano letters, 2016, vol. 16, no. 4, pp. 2159–2167. https://doi.org/10.1021/acs.nanolett.5b03901

[27] Y.-Y. Li, J.-G. Wang, X.-R. Liu, C. Shen, K. Xie and B. Wei, *Au/TiO$_2$ hollow spheres with synergistic effect of plasmonic enhancement and light scattering for improved dye-sensitized solar cells*, ACS Applied Materials and Interfaces, 2017, vol. 9, no. 37, pp. 31691–31698. https://doi.org/10.1021/acsami.7b04624

[28] J. Liang, H. Liu, J. Yu, L. Zhou and J. Zhu, *Plasmon-enhanced solar vapor generation*, Nanophotonics, 2019, vol. 8, no. 5, pp. 771–786. https://doi.org/10.1515/nanoph-2019-0039

[29] F.-X. Liang, C.-W. Ge, T.-F. Zhang, W.-J. Xie, D.-Y. Zhang, Y.-F. Zou, K. Zheng and L.-B. Luo, *Plasmonic hollow gold nanoparticles induced high-performance Bi$_2$S$_3$ nanoribbon photodetector*, Nanophotonics, 2017, vol. 6, no. 2, pp. 494–501. https://doi.org/10.1515/nanoph-2016-0024

[30] X.D. Gao, G.T. Fei, S.H. Xu, B.N. Zhong, H.M. Ouyang, X.H. Li and L.D. Zhang, *Porous Ag/TiO$_2$-Schottky-diode based plasmonic hot-electron photodetector with high detectivity and fast response*, Nanophotonics, 2019, vol. 8, no. 7, pp. 1247–1254. https://doi.org/10.1515/nanoph-2019-0094

[31] J. You, Y. Yu, K. Cai, D. Zhou, H. Zhu, R. Wang, Q. Zhang, H. Liu, Y. Cai, D. Lu, J.-K. Kim, L. Gan, T. Zhai and Z. Luo, *Enhancement of MoTe$_2$ near-infrared absorption with gold hollow nanorods for photodetection*, Nano Research, 2020, vol. 13, pp. 1636–1643. https://doi.org/10.1007/s12274-020-2786-9

[32] X. Liu, J. Lin, T.F. Jiang, Z.F. Zhu, Q.Q. Zhan, J. Qian and S. He, Surface plasmon properties of hollow AuAg alloyed triangular nanoboxes and its applications in SERS imaging and potential drug delivery, Progress in Electromagnetics Research, 2012, vol. 128, pp. 35–53. http://doi.org/10.2528/PIER12041908

[33] Z. Hu, C.S. Meduri, R.S.J. Ingrole, H.S. Gill and G. Kumar, *Solid and hollow metallic glass microneedles for transdermal drug-delivery*, Applied Physics Letters, 2020, vol. 116, no. 20, art. no. 203703. https://doi.org/10.1063/5.0008983

[34] X. Yu, K. Yang, X. Chen and W. Li, *Black hollow silicon oxide nanoparticles as highly efficient photothermal agents in the second near-infrared window for in vivo cancer therapy*, Biomaterials, 2017, vol. 143, pp. 120–129. https://doi.org/10.1016/j.biomaterials.2017.07.037

[35] W. Liu, X. Li, W. Li, Q. Zhang, H. Bai, J. Li and G. Xi, *Highly stable molybdenum dioxide nanoparticles with strong plasmon resonance are promising in photothermal cancer therapy*, Biomaterials, 2018, vol. 163, pp. 43–54. https://doi.org/10.1016/j.biomaterials.2018.02.021

[36] E. Yasun, S. Gandhi, S. Choudhury, R. Mohammadinejad, F. Benyettou, N. Gozubenli and H. Arami, *Hollow micro and nanostructures for therapeutic and imaging applications*, Journal of Drug Delivery Science and Technology, 2020, vol. 60, art. no. 102094. https://doi.org/10.1016/j.jddst.2020.102094

[37] X. Wei, X. He, P. Wu, F. Gong, D. Wang, S. Wang, S. Lu, J. Zhang, S. Xiang, T. Kai and P. Ding, *Recent advances in the design of semiconductor hollow microspheres for enhanced photocatalytic water splitting*, International Journal of Hydrogen Energy, 2021, vol. 46, no. 55, pp. 27974–27996. https://doi.org/10.1016/j.ijhydene.2021.06.076

[38] B. Fang, Z. Xing, D. Sun, Z. Li and W. Zhou, *Hollow semiconductor photocatalysts for solar energy conversion*, Advanced Powder Materials, 2021, vol. 1, no. 2, art. no. 100021. https://doi.org/10.1016/j.apmate.2021.11.008

[39] P. Zhang, S. Wang, B.Y. Guan and X.W.D. Lou, *Fabrication of CdS hierarchical multi-cavity hollow particles for efficient visible light CO$_2$ reduction*, Energy and Environmental Science, 2019, vol. 12, no. 1, pp. 164–168. https://doi.org/10.1039/C8EE02538J

[40] Z. Wang, S.A. Monny and L. Wang, *Hollow structure for photocatalytic CO$_2$ reduction*, ChemNanoMat, 2020, vol. 6, no. 6, pp. 881–888. https://doi.org/10.1002/cnma.202000157

[41] X. Wang, S.-I. Choi, L.T. Roling, M. Luo, C. Ma, L. Zhang, M. Chi, J. Liu, Z. Xie, T.A. Herron, M. Mavrikakis and Y. Xia, *Palladium–platinum core-shell icosahedra with substantially enhanced activity and durability towards oxygen reduction*, Nature Communications, 2015, vol. 6, art. no. 7594. https://doi.org/10.1038/ncomms8594

[42] X. Wang, M. Vara, M. Luo, H. Huang, A. Ruditskiy, J. Park, S. Bao, J. Liu, J. Howe, M. Chi, Z. Xie and Y. Xia, *Pd@Pt core-shell concave decahedra: a class of catalysts for the oxygen reduction reaction with enhanced activity and durability*, Journal of the American Chemical Society, 2015, vol. 137, no. 47, pp. 15036–15042. https://doi.org/10.1021/jacs.5b10059

[43] D.S. He, D. He, J. Wang Y. Lin, P. Yin, X. Hong, Y. Wu and Y. Li, *Ultrathin icosahedral Pt-enriched nanocage with excellent oxygen reduction reaction activity*, Journal of the American Chemical Society, 2016, vol. 138, no. 5, pp. 1494-1497. https://doi.org/10.1021/jacs.5b12530

[44] M. Zhao, L. Xu, M. Vara, A.O. Elnabawy, K.D. Gilroy, Z.D. Hood, S. Zhou, L. Figueroa-Cosme, M. Chi, M. Mavrikakis and Y. Xia, *Synthesis of Ru icosahedral nanocages with a face-centered-cubic structure and evaluation of their catalytic properties*, ACS Catalysis, 2018, vol. 8, no. 8, pp. 6948–6960. https://doi.org/10.1021/acscatal.8b00910

[45] C.-T. Lee, H. Wang, M. Zhao, T.-H. Yang, M. Vara and Y. Xia, *One-pot synthesis of Pd@Pt$_{nL}$ core-shell icosahedral nanocrystals in high throughput through a quantitative analysis of the reduction kinetics*, Chemistry – A European Journal, 2019, vol. 25, no. 20, pp. 5322–5329. https://doi.org/10.1002/chem.201900229

[46] H. Tian, H. Tian, W. Yang, F. Zhang, W. Yang, Q. Zhang, Y. Wang, J. Liu, S.R.P. Silva, H. Liu and G. Wang, *Stable hollow-structured silicon suboxide-based anodes toward high-performance lithium-ion batteries*, Advanced Functional Materials, 2021, vol. 31, no. 25, art. no. 2101796. https://doi.org/10.1002/adfm.202101796

[47] X.-S. Tao, Y.-G. Sun, Y. Liu, B.-B. Chang, C.-T. Liu, Y.-S. Xu, X.-C. Yang and A.-M Cao,

Facile synthesis of hollow carbon nanospheres and their potential as stable anode materials in potassium-ion batteries, ACS Applied Materials and Interfaces, 2020, vol. 12, no. 11, pp. 13182–13188. https://doi.org/10.1021/acsami.9b22736

[48] X.-H. Liu, W.-H. Lai and S.-L. Chou, *The application of hollow micro-/nanostructured cathodes for sodium-ion batteries*, Materials Chemistry Frontiers, 2020, vol. 4, no. 5, pp. 1289–1303. https://doi.org/10.1039/C9QM00674E

[49] Z. Li, H.B. Wu and X.W. Lou, *Rational designs and engineering of hollow micro-/nanostructures as sulfur hosts for advanced lithium-sulfur batteries*, Energy and Environmental Science, 2016, vol. 9, no. 10, pp. 3061–3070. https://doi.org/10.1039/C6EE02364A

[50] A. Gong, Y. Zhao, B. Liang and K. Li, *Stepwise hollow Prussian blue/carbon nanotubes composite as a novel electrode material for high-performance desalination*, Journal of Colloid and Interface Science, 2022, vol. 605, pp. 432–440. https://doi.org/10.1016/j.jcis.2021.07.103

[51] S. Biswas, V. Sharma, D. Mandal, A. Chowdhury, M. Chakravarty, S. Priya, C.C. Gowda, P. De, I. Singh and A. Chandra, *Hollow nanostructures of metal oxides as emerging electrode materials for high performance supercapacitors*, CrystEngComm, 2020, vol. 22, no. 9, pp. 1633–1644. https://doi.org/10.1039/C9CE01547G

[52] M. Zhu, Y. Cheng, Q. Luo, M. El-khateeb and Q. Zhang, *A review of synthetic approaches to hollow nanostructures*, Materials Chemistry Frontiers, 2021, vol. 5, no. 6, pp. 2552–2587. https://doi.org/10.1039/D0QM00879F

[53] S.F. Soares, T. Fernande, A.L. Daniel-da-Silva and T. Trindade, *The controlled synthesis of complex hollow nanostructures and prospective applications*, Proceedings of the Royal Society A, 2019, vol. 475, no. 2224, art. no. 20180677. https://doi.org/10.1098/rspa.2018.0677

[54] J. Feng and Y. Yin, *Self-templating approaches to hollow nanostructures*, Advanced Materials, 2019, vol. 31, no. 38, art. no. 1802349. https://doi.org/10.1002/adma.201802349

[55] L. Yu, X.Y. Yu and X.W. Lou, *The design and synthesis of hollow micro-/nanostructures: Present and future trends*, Advanced Materials, 2018, vol. 30, no. 38, art. no. 1800939. https://doi.org/10.1002/adma.201800939

[56] X. Wang, J.I. Feng, Y. Bai, Q. Zhang and Y. Yin, *Synthesis, properties, and applications of hollow micro-/nanostructures*, Chemical Reviews, 2016, vol. 116, no. 18, pp. 10983–11060. https://doi.org/10.1021/acs.chemrev.5b00731

[57] X.W. Lou, L.A. Archer and Z. Yang, *Hollow micro-/nanostructures: synthesis and applications*, Advanced Materials, 2008, vol. 20, no. 21, pp. 3987–4019. https://doi.org/10.1002/adma.200800854

[58] Y. Sun, B.T. Mayers and Y. Xia, *Template-engaged replacement reaction: a one-step approach to the large-scale synthesis of metal nanostructures with hollow interiors*, Nano Letters, 2002, vol. 2, no. 5, pp. 481–485. https://doi.org/10.1021/nl025531v

[59] A.-A. El Mel, R. Nakamura and C. Bittencourt, *The Kirkendall effect and nanoscience: hollow nanospheres and nanotubes*, Beilstein Journal of Nanotechnology, 2015, vol. 6, pp. 1348–1361. https://doi.org/10.3762/bjnano.6.139

[60] H.J. Fan, U. Gösele and M. Zacharias, *Formation of nanotubes and hollow nanoparticles based on Kirkendall and diffusion processes: a review*, Small, 2007, vol 3, no. 10, pp. 1660–1671. https://doi.org/10.1002/smll.200700382

[61] F. Merkoçi, J. Patarroyo, L. Russo, J. Piella, A. Genç, J. Arbiol, N.G. Bastús and V. Puntes, *Understanding galvanic replacement reactions: the case of Pt and Ag*, Materials Today Advances, 2020, vol. 5, art. no. 100037. https://doi.org/10.1016/j.mtadv.2019.100037

[62] M. Ibáñez, J. Fan, W. Li, D. Cadavid, R. Nafria, A. Carrete and A. Cabot, *Means and limits of control of the shell parameters in hollow nanoparticles obtained by the Kirkendall effect*, Chemistry of Materials, 2011, vol. 23, no. 12, pp. 3095–3104. https://doi.org/10.1021/cm2006633

[63] B.D. Anderson and J.B. Tracy, *Nanoparticle conversion chemistry: Kirkendall effect, galvanic exchange, and anion exchange*, Nanoscale, 2014, vol. 6, no. 21, pp. 12195–12216. https://doi.org/10.1039/C4NR02025A

[64] Z. Yang, N. Yang and M.-P. Pileni, *Nano Kirkendall effect related to nanocrystallinity of metal nanocrystals: influence of the outward and inward atomic diffusion on the final nanoparticle structure*, The Journal of Physical Chemistry C, 2015, vol. 119, no. 39, pp. 22249–22260. https://doi.org/10.1021/acs.jpcc.5b06000

[65] G. Glodán, C. Cserháti, I. Beszeda and D.L. Beke, *Production of hollow hemisphere shells by pure Kirkendall porosity formation in Au/Ag system*,

Applied Physics Letters, 2010, vol. 97, no. 11, art. no. 113109. https://doi.org/10.1063/1.3490675

[66] A.E. Paz y Puente, D. Erdeniz, J.L. Fife and D.C. Dunand, *In situ X-ray tomographic microscopy of Kirkendall pore formation and evolution during homogenization of pack-aluminized Ni-Cr wires*, Acta Materialia, 2016, vol. 103, pp. 534–546. https://doi.org/10.1016/j.actamat.2015.10.013

[67] M. Bobeth, M. Gutkin, W. Pompe and A.E. Romanov, *Modelling of vacancy diffusion and pore formation during parabolic oxide growth*, Physica Status Solidi (a), 1998, vol. 165, no. 1, pp. 165–184. https://doi.org/10.1002/(SICI)1521-396X (199801)165:1%3C165::AID-PSSA165%3 E3.0.CO;2-U

[68] A.D. Brailsford and R. Bullough, *The theory of sink strengths*, Philosophical Transactions of the Royal Society of London. Series A, Mathematical and Physical Sciences, 1981, vol. 302, no.1465, pp. 87–137. https://doi.org/10.1098/rsta.1981.0158

[69] R. Bullough and R.C. Newman, *The kinetics of migration of point defects to dislocations*, Reports on Progress in Physics, 1970, vol. 33, no. 1, art. no. 101. https://doi.org/10.1088/0034-4885/33/1/303

[70] M. Vara, X. Wang, J. Howe, M. Chi and Y. Xia, *Understanding the stability of Pt-based nanocages under thermal stress using in situ electron microscopy*, ChemNanoMat, 2018, vol. 4, no. 1, pp. 112–117. https://doi.org/10.1002/cnma.201700298

[71] J. Park, H. Zheng, Y. Jun and A.P. Alivisatos, *Hetero-epitaxial anion exchange yields single-crystalline hollow nanoparticles*, Journal of the American Chemical Society, 2009, vol. 131, no. 39, pp. 13943–13945. https://doi.org/10.1021/ja905732q

[72] K.N. Tu and U. Gösele, *Hollow nanostructures based on the Kirkendall effect: design and stability considerations*, Applied Physics Letters, 2005, vol. 86, no. 9, art. no. 093111. https://doi.org/10.1063/1.1873044

[73] F. Güder, Y. Yang, S. Goetze, A. Berger, N. Ramgir, D. Hesse and M. Zacharias, *Controlled positioning of large interfacial nanocavities via stress-engineered void localization*, Small, 2010, vol. 6, no. 15, pp. 1603–1607. https://doi.org/10.1002/smll.201000561

[74] I.V. Belova, A.V. Evteev, E.V. Levchenko and G.E. Murch, *The synthesis, stability and shrinkage of hollow nanoparticles: an overview*, Journal of Nano Research, 2009, vol. 7, pp. 19–26. https://doi.org/10.4028/www.scientific.net/ JNanoR.7.19

[75] G.E. Murch, A.V. Evteev, E.V. Levchenko and I.V. Belova, *Recent progress in the simulation of diffusion associated with hollow and Bi-metallic nanoparticles*, Diffusion Fundamentals, 2009, vol. 11, no. 42, pp. 1–22. http://ul.qucosa.de/fileadmin/data/qucosa/documents/18982/diff_fund_11%282009%2942.pdf

[76] A.M. Gusak, T.V. Zaporozhets, Y.O. Lyashenko, S.V. Kornienko, M.O. Pasichnyy and A.S. Shirinyan, *Diffusion-controlled solid state reactions: in alloys, thin films and nanosystems*, John Wiley and Sons, 2010.

[77] T.V. Zaporozhets, A.M. Gusak and O.M. Podolyan, *Evolution of pores in nanoshells — a competition of direct and inverse Kirkendale effects, Frenkel and Gibbs–Thomson effects: the phenomenological description and computer simulation*, Usp. Fiz. Met., 2012, vol. 13, no. 1, pp. 1–70 (in Russian). https://doi.org/10.15407/ufm.13.01.001

[78] J.M. Gac, *Numerical modelling of formation of highly ordered structured micro- and nanoparticles – A review*, KONA Powder and Particle Journal, 2022, vol. 39, pp. 45–61. https://doi.org/10.14356/kona.2022019

[79] R. Nakamura, D. Tokozakura, J.-G. Lee, H. Mori and H. Nakajima, *Shrinking of hollow Cu_2O and NiO nanoparticles at high temperatures*, Acta Materialia, 2008, vol. 56, no. 18, pp. 5276–5284. https://doi.org/10.1016/j.actamat.2008.07.004

[80] R. Nakamura, G. Matsubayashi, H. Tsuchiya, S. Fujimoto and H. Nakajima, *Formation of oxide nanotubes via oxidation of Fe, Cu and Ni nanowires and their structural stability: Difference in formation and shrinkage behavior of interior pores*, Acta Materialia, 2009, vol. 57, no. 17, pp. 5046–5052. https://doi.org/10.1016/j.actamat.2009.07.006

[81] G. Glodán, C. Cserháti and D.L. Beke, *Temperature-dependent formation and shrinkage of hollow shells in hemispherical Ag/Pd nanoparticles*, Philosophical Magazine, 2012, vol. 92, no. 31, pp. 3806–3812. https://doi.org/10.1080/14786435.2012.687841

[82] S. Chenna and P.A. Crozier, *In situ environmental transmission electron microscopy to determine transformation pathways in supported Ni nanoparticles*, Micron, 2012, vol. 43, no. 11,

pp. 1188–1194.
https://doi.org/10.1016/j.micron.2012.04.007

[83] J.A. Medford, A.C. Johnston-Peck and J.B. Tracy, *Nanostructural transformations during the reduction of hollow and porous nickel oxide nanoparticles*, Nanoscale, 2013, vol. 5, no. 1, pp. 155–159. https://doi.org/10.1039/C2NR33005A

[84] A.M. Gusak, T.V. Zaporozhets, K.N. Tu and U. Gösele, *Kinetic analysis of the instability of hollow nanoparticles,* Philosophical Magazine, 2005, vol. 85, no. 36, pp. 4445–4464. https://doi.org/10.1080/14786430500311741

[85] A.V. Evteev, E.V. Levchenko, I.V. Belova and G.E. Murch, *Formation of a hollow binary alloy nanosphere: a kinetic Monte Carlo study*, Journal of Nano Research, 2009, vol. 7, pp. 11–17. https://doi.org/10.4028/www.scientific.net/JNanoR.7.11

[86] L. Jiang, X. Yin, J. Zhao, H. Liu, Y. Liu, F. Wang, J. Zhu, F. Boey and H. Zhang, *Theoretical investigation on the thermal stability of hollow gold nanoparticles*, The Journal of Physical Chemistry C, 2009, vol. 113, no. 47, pp. 20193–20197. https://doi.org/10.1021/jp905280g

[87] S. Jiang, Y. Zhang, Y. Gan, Z. Chen and H. Peng, *Molecular dynamics study of neck growth in laser sintering of hollow silver nanoparticles with different heating rates*, Journal of Physics D: Applied Physics, 2013, vol. 46, no. 33, art. no. 335302. https://doi.org/10.1088/0022-3727/46/33/335302

[88] Y. Wang, Q. Liu, Y. Sun and R. Wang, *Magnetic field modulated SERS enhancement of CoPt hollow nanoparticles with sizes below 10 nm*, Nanoscale, 2018, vol. 10, no. 26, pp. 12650–12656. https://doi.org/10.1039/C8NR03781G

[89] M.A. Ratner and V.V. Yanovsky, *Magic pore dynamics in weakly interacting clusters*, 2020, arXiv preprint, arXiv:2001.11209. https://doi.org/10.48550/arXiv.2001.11209

[90] F.J. Valencia, M. Ramírez, A. Varas and J. Rogan, *Understanding the stability of hollow nanoparticles with polycrystalline shells*, The Journal of Physical Chemistry C, 2020, vol. 124, no. 18, pp. 10143–10149. https://doi.org/10.1021/acs.jpcc.0c00258

[91] F.J. Valencia, M. Ramírez, A. Varas, J. Rogan and M. Kiwi, *Thermal stability of hollow porous gold nanoparticles: A molecular dynamics study*, Journal of Chemical Information and Modeling, 2020, vol. 60, no. 12, pp. 6204–6210. https://doi.org/10.1021/acs.jcim.0c00785

[92] G. Ferbonink, T.S. Rodrigues, P. Camargo, R. Albuquerque and R. Nome, *Stochastic thermodynamics analysis of ultrafast AgAu nanoshell dynamics in the nonlinear response regime*, 2020, ChemRxiv preprint. https://doi.org/10.26434/chemrxiv.12846695.v1

[93] C. Jiang, Y. Mo, H. Wang, R. Li, M. Huang and S. Jiang, *Molecular dynamics simulation of the production of hollow silver nanoparticles under ultrafast laser irradiation*, Computational Materials Science, 2021, vol. 196, art. no. 110545. https://doi.org/10.1016/j.commatsci.2021.110545

[94] J.P. Hirth, J. Lothe, *Theory of dislocations,* 2nd edition, Wiley, New York, 1982.

[95] A.V. Evteev, E.V. Levchenko, I.V. Belova and G.E. Murch, *Shrinking kinetics by vacancy diffusion of a pure element hollow nanosphere*, Philosophical Magazine, 2007, vol. 87, no. 25, pp. 3787–3796. https://doi.org/10.1080/14786430601103005

[96] V.V. Yanovsky, M.I. Kopp and M.A. Ratner, *Evolution of vacancy pores in bounded particles,* 2018, arXiv preprint, arXiv:1809.06565. https://doi.org/10.48550/arXiv.1809.06565

[97] V.V. Yanovsky, M.I. Kopp and M.A. Ratner, *Evolution of gas-filled pore in bounded particles*, 2018, arXiv preprint, arXiv:1810.10319. https://doi.org/10.48550/arXiv.1810.10319

[98] V.V. Yanovsky, M.I. Kopp and M.A. Ratner, *Gas-filled pore in bounded particle*, 2019, arXiv preprint, arXiv:1910.13956. https://doi.org/10.48550/arXiv.1910.13956

[99] L. Klinger, G.E. Murch, I.V. Belova and E. Rabkin, *Pores shrinkage and growth in polycrystalline hollow nanoparticles and nanotubes*, Scripta Materialia, 2020, vol. 180, pp. 93–96. https://doi.org/10.1016/j.scriptamat.2020.01.029

[100] O.M. Podolyan and T.V. Zaporozhets, *Void formation and collapse in nanowires*, Ukrainian Journal of Physics, 2011, vol. 56, no. 9, pp. 929–939. https://doi.org/10.15407/ujpe56.9.929

[101] Y. Yin, C.K. Erdonmez, A. Cabot, S. Hughes and A.P. Alivisatos, *Colloidal synthesis of hollow cobalt sulfide nanocrystals*, Advanced Functional Materials, 2006, vol. 16, no. 11, pp. 1389–1399. https://doi.org/10.1002/adfm.200600256

[102] R.A. Masumura, B.B. Rath and C.S. Pande, *Analysis of Cu-Ni diffusion in a spherical geometry for excess vacancy production*, Acta Materialia, 2002, vol. 50, no.18, pp. 4535–4544. https://doi.org/10.1016/S1359-6454(02)00273-2

[103] S. Prasad and A. Paul, *Theoretical consideration on the formation of nanotube following the Kirkendall effect*, Applied Physics Letters, 2007,

vol. 90, no. 23, art. no. 233114. https://doi.org/10.1063/1.2747184

[104] H.-C. Yu, D.-H. Yeon, X. Li and K. Thornton, *Continuum simulations of the formation of Kirkendall-effect-induced hollow cylinders in a binary substitutional alloy*, Acta Materialia, 2009, vol. 57, no. 18, pp. 5348–5360. https://doi.org/10.1016/j.actamat.2009.07.033

[105] S. Jana, J.W. Chang and R.M. Rioux, *Synthesis and modeling of hollow intermetallic Ni–Zn nanoparticles formed by the Kirkendall effect*, Nano Letters, 2013, vol. 13, no. 8, pp. 3618–3625. https://doi.org/10.1021/nl401467r

[106] V.I. Levitas and H. Attariani, *Mechanochemical continuum modeling of nanovoid nucleation and growth in reacting nanoparticles*, The Journal of Physical Chemistry C, 2012, vol. 116, no. 1, pp. 54–62. https://doi.org/10.1021/jp2055365

[107] L. Klinger, O. Kraft and E. Rabkin, *A model of Kirkendall hollowing of core-shell nanowires and nanoparticles controlled by short-circuit diffusion*, Acta Materialia, 2015, vol. 83, pp. 180–186. https://doi.org/10.1016/j.actamat.2014.09.050

[108] J. Svoboda, I. Turek and F.D. Fischer, *Application of the thermodynamic extremal principle to modeling of thermodynamic processes in material sciences*, Philosophical Magazine, 2005, vol. 85, no. 31, pp. 3699–3707. https://doi.org/10.1080/14786430500267760

[109] J. Svoboda, E. Gamsjäger and F.D. Fischer, *Relaxation of the elastic strain energy of misfitting inclusions due to diffusion of vacancies*, Philosophical Magazine Letters, 2005, vol. 85, no. 9, pp. 473–479. https://doi.org/10.1080/09500830500333295

[110] F.D. Fischer, K. Hackl and J. Svoboda, *Improved thermodynamic treatment of vacancy-mediated diffusion and creep*, Acta Materialia, 2016, vol. 108, pp. 347–354. https://doi.org/10.1016/j.actamat.2016.01.017

[111] F.D. Fischer and J. Svoboda, *High temperature instability of hollow nanoparticles*, Journal of Nanoparticle Research, 2008, vol. 10, no. 2, pp. 255–261. https://doi.org/10.1007/s11051-007-9242-6

[112] J. Svoboda, F.D. Fischer and D. Vollath, *Modeling of formation of binary-phase hollow nanospheres from metallic solid nanospheres*, Acta Materialia, 2009, vol. 57, no. 6, pp. 1912–1919. https://doi.org/10.1016/j.actamat.2008.12.038

[113] F.D. Fischer and J. Svoboda, *Modelling of reaction of metallic nanospheres with gas*, Solid State Phenomena, 2011, vols. 172–174,

pp. 1028–1037. https://doi.org/10.4028/www.scientific.net/SSP.172-174.1028

[114] Y. Watanabe, R.W. Mowbray, K.P. Rice and M.P. Stoykovich, *Kinetic description of metal nanocrystal oxidation: a combined theoretical and experimental approach for determining morphology and diffusion parameters in hollow nanoparticles by the nanoscale Kirkendall effect*, Philosophical Magazine, 2014, vol. 94, no. 30, pp. 3487–3506. https://doi.org/10.1080/14786435.2014.962640

[115] M. Luo, A. Ruditskiy, H.-C. Peng, J. Tao, L. Figueroa-Cosme, Z. He and Y. Xia, *Pentatwinned copper nanorods: facile synthesis via seed-mediated growth and their tunable plasmonic properties*, Advanced Functional Materials, 2016, vol. 26, no. 8, pp. 1209–1216. https://doi.org/10.1002/adfm.201504217

[116] L.D. Marks and L. Peng, *Nanoparticle shape, thermodynamics and kinetics*, Journal of Physics: Condensed Matter, 2016, vol. 28, no. 5, art. no. 053001. https://doi.org/10.1088/0953-8984/28/5/053001

[117] H. Wang, S. Zhou, K.D. Gilroy, Z. Cai and Y. Xia, *Icosahedral nanocrystals of noble metals: synthesis and applications*, Nano Today, 2017, vol. 15, pp. 121–144. https://doi.org/10.1016/j.nantod.2017.06.011

[118] S. Zhou, M. Zhao, T.-H. Yang and Y. Xia, *Decahedral nanocrystals of noble metals: synthesis, characterization, and applications*, Materials Today, 2019, vol. 22, pp. 108–131. https://doi.org/10.1016/j.mattod.2018.04.003

[119] C.L. Johnson, E. Snoeck, M. Ezcurdia, B. Rodríguez-González, I. Pastoriza-Santos, L.M. Liz-Marzán and M.J. Hÿtch, *Effects of elastic anisotropy on strain distributions in decahedral gold nanoparticles*, Nature Materials, 2008, vol. 7, no. 2, pp. 120–124. https://doi.org/10.1038/nmat2083

[120] M.J. Walsh, K. Yoshida, A. Kuwabara, M.L. Pay, P.L. Gai and E.D. Boyes, *On the structural origin of the catalytic properties of inherently strained ultrasmall decahedral gold nanoparticles*, Nano Letters, 2012, vol. 12, no. 4, pp. 2027–2031. https://doi.org/10.1021/nl300067q

[121] B. Goris, J. De Beenhouwer, A. De Backer, D. Zanaga, K.J. Batenburg, A. Sánchez-Iglesias, L.M. Liz-Marzán, S. Van Aert, S. Bals, J. Sijbers and G. Van Tendeloo, *Measuring lattice strain in three dimensions through electron*

microscopy, Nano Letters, 2015, vol. 15, no. 10, pp. 6996–7001.
https://doi.org/10.1021/acs.nanolett.5b03008

[122] A.E. Romanov and V.I. Vladimirov, *Disclinations in crystalline solids*, in: F.R.N. Nabarro (ed.), *Dislocations in Solids*, vol. 9., North-Holland Publ. Co, Amsterdam, pp. 191–402, 2010.

[123] A.E. Romanov and A.L. Kolesnikova, *Application of disclination concept to solid structures*, Progress in Materials Science, 2009, vol. 54, no. 6, pp. 740–769.
https://doi.org/10.1016/j.pmatsci.2009.03.002

[124] R. De Wit, *Partial disclinations*, Journal of Physics C: Solid State Physics, 1972, vol. 5, pp. 529–534.
https://doi.org/10.1088/0022-3719/5/5/004

[125] J.M. Galligan, *Fivefold symmetry and disclinations*, Scripta Metallurgica, 1972, vol. 6, no. 2, pp. 161–163.
https://doi.org/10.1016/0036-9748(72)90269-4

[126] H. Hofmeister, A.F. Bardamid, T. Junghanns and S.A. Nepijko, *Crystalline particles with multiply twinned structure in amorphous films of germanium*, Thin Solid Films, 1991, vol. 205, no. 1, pp. 20–24.
https://doi.org/10.1016/0040-6090(91)90463-8

[127] I.A. Polonsky, A.E. Romanov, V.G. Gryaznov and A.M. Kaprelov, *Disclination in an elastic sphere*, Philosophical Magazine A, 1991, vol. 64, no. 2, pp. 281–287.
https://doi.org/10.1080/01418619108221185

[128] A.E. Kolesnikova, M.Yu. Gutkin, A.V. Proskura, N.F. Morozov and A.E. Romanov, *Elastic fields of straight wedge disclinations axially piercing bodies with spherical free surfaces*, International Journal of Solids Structures, 2016, vol. 99, pp. 82–96.
https://doi.org/10.1016/j.ijsolstr.2016.06.029

[129] A. Howie and L.D. Marks, *Elastic strains and the energy balance for multiply twinned particles*, Philosophical Magazine A, 1984, vol. 49, no. 1, pp. 95–109.
https://doi.org/10.1080/01418618408233432

[130] A.E. Romanov, I.A. Polonsky, V.G. Gryaznov, S.A. Nepijko, T. Junghanns and N.J. Vitrykhovski, *Voids and channels in pentagonal crystals*, Journal of Crystal Growth, 1993, vol. 129, pp. 691–698.
https://doi.org/10.1016/0022-0248(93)90505-Q

[131] I.S. Yasnikov and A.A. Vikarchuk, *Evolution of the formation and growth of a cavity in pentagonal crystals of electrolytic origin*, Physics of the Solid State, 2006, vol. 48, no. 8, pp. 1433–1438.
https://doi.org/10.1134/S1063783406080026

[132] I.S. Yasnikov and A.A. Vikarchuk, *Voids in icosahedral small particles of an electrolytic metal*, JETP Letters, 2006, vol. 83, no. 1, pp. 42–45.
https://doi.org/10.1134/S0021364006010103

[133] I.S. Yasnikov, *Mechanism of the formation of cavities in icosahedral metallic small particles of electrolytic origin*, Physics of the Solid State, 2007, vol. 49, no. 7, pp. 1224–1228.
https://doi.org/10.1134/S1063783407070049

[134] J. Huang, Y. Yan, X. Li, X. Qiao, J. Wu, J. Li and H. Zhang, *Unexpected Kirkendall effect in twinned icosahedral nanocrystals driven by strain gradient*, Nano Research, 2020, vol. 13, no. 10, pp. 2641–2649.
https://doi.org/10.1007/s12274-020-2903-9

[135] X. Wang, L. Figueroa-Cosme, X. Yang, M. Luo, J. Liu, Z. Xie and Y. Xia, *Pt-based icosahedral nanocages: using a combination of {111} facets, twin defects, and ultrathin walls to greatly enhance their activity toward oxygen reduction*, Nano Letters, 2016, vol. 16, no. 2, pp. 1467–1471.
https://doi.org/10.1021/acs.nanolett.5b05140

[136] L. Han, P. Xiong, J. Bai and S. Che, *Spontaneous formation and characterization of silica mesoporous crystal spheres with reverse multiply twinned polyhedral hollows*, Journal of the American Chemical Society, 2011, vol. 133, no. 16, pp. 6106–6109.
https://doi.org/10.1021/ja110443a

[137] Y. Sun and Y. Xia, *Multiple-walled nanotubes made of metals*, Advanced Materials, 2004, vol. 16, no. 3, pp. 264–268.
https://doi.org/10.1002/adma.200305780

[138] Z. Jiang, Q. Zhang, C. Zong, B.-J. Liu, B. Ren, Z. Xie and L. Zheng, *Cu-Au alloy nanotubes with five-fold twinned structure and their application in surface-enhanced Raman scattering*, Journal of Materials Chemistry, 2012, vol. 22, no. 35, pp. 18192–18197.
https://doi.org/10.1039/C2JM33863G

[139] H.M. Song, D.H. Anjum, R. Sougrat, M.N. Hedhili and N.M. Khashab, *Hollow Au@Pd and Au@Pt core-shell nanoparticles as electrocatalysts for ethanol oxidation reactions*, Journal of Materials Chemistry, 2012, vol. 22, no. 48, pp. 25003–25010.
https://doi.org/10.1039/C2JM35281H

[140] P. Hou, P. Cui, H. Liu, J. Li and J. Yang, *Nanoscale noble metals with a hollow interior formed through inside-out diffusion of silver in solid-state core-shell nanoparticles*, Nano

Research, 2015, vol. 8, no. 2, pp. 512–522.
https://doi.org/10.1007/s12274-014-0663-0

[141] H. Huang, L. Zhang, T. Lv, A. Ruditskiy, J. Liu, Z. Ye and Y. Xia, *Five-fold twinned Pd nano-rods and their use as templates for the synthesis of bimetallic or hollow nanostructures*, ChemNanoMat, 2015, vol. 1, no. 4, pp. 246–252. https://doi.org/10.1002/cnma.201500042

[142] Z. Fang, Y. Wang, C. Liu, S. Chen, W. Sang, C. Wang and J. Zeng, *Rational design of metal nanoframes for catalysis and plasmonics*, Small, 2015, vol. 11, no. 22, pp. 2593–2605. https://doi.org/10.1002/smll.201402799

[143] S. Tehuacanero-Cuapa, R. Palomino-Merino and J. Reyes-Gasga, *CBED electron beam drilling and closing of holes in decahedral silver nano-particles*, Radiation Physics and Chemistry, 2013, vol. 87, pp. 59–63. https://doi.org/10.1016/j.radphyschem.2013.02.023

[144] S. Tehuacanero-Cuapa, J. Reyes-Gasga, E.F. Brès, R. Palomino-Merino and R. García-García, *Holes drilling in gold and silver decahedral nanoparticles by the convergent beam electron diffraction electron beam*, Radiation Effects and Defects in Solids, 2014, vol. 169, no. 10, pp. 838–844. https://doi.org/10.1080/10420150.2014.958747

[145] S. Tehuacanero-Cuapa, J. Reyes-Gasga, A. Rodríguez-Gómez, D. Bahena, I. Hernández-Calderón and R. García-García, *The low-loss EELS spectra from radiation damaged gold na-noparticles*, Journal of Applied Physics, 2016, vol. 120, no. 16, art. no. 164302. https://doi.org/10.1063/1.4965862

[146] A.L. Kolesnikova and A.E. Romanov, *Stress re-laxation in pentagonal whiskers*, Technical Phys-ics Letters, 2007, vol. 33, no. 10, pp. 886–888. https://doi.org/10.1134/S1063785007100239

[147] M.Yu. Gutkin, A.L. Kolesnikova, S.A. Kras-nitckii, L.M. Dorogin, V.S. Serebryakova, A.A. Vikarchuk and A.E. Romanov, *Stress re-laxation in icosahedral small particles via gen-eration of circular prismatic dislocation loops*, Scripta Materialia, 2015, vol. 105, pp. 10–13. https://doi.org/10.1016/j.scriptamat.2015.04.015

[148] M.Yu. Krauchanka, S.A. Krasnitckii, M.Yu. Gutkin, A.L. Kolesnikova, A.E. Roma-nov and E.C. Aifantis, *Generation of circular prismatic dislocation loops in decahedral small particles*, Scripta Materialia, 2018, vol. 146, pp. 77–81. https://doi.org/10.1016/j.scriptamat.2017.11.006

[149] M.Yu. Gutkin, A.L. Kolesnikova, S.A. Krasnit-sky, and A.E. Romanov, *Misfit dislocation loops*

in composite core-shell nanoparticles, Physics of the Solid State, 2014, vol. 56, no. 4, pp. 723–730. https://doi.org/10.1134/S1063783414040106

[150] M.Yu. Gutkin, A.L. Kolesnikova, S.A. Kras-nitckii, A.E. Romanov and A.G. Shalkovskii, *Misfit dislocation loops in hollow core-shell na-noparticles*, Scripta Materialia, 2014, vol. 83, pp. 1–4. https://doi.org/10.1016/j.scriptamat.2014.03.005

[151] M.Yu. Krauchanka, S.A. Krasnitckii, M.Yu. Gutkin, A.L. Kolesnikova and A.E. Romanov, *Circular loops of misfit disloca-tions in decahedral core-shell nanoparticles*, Scripta Materialia, 2019, vol. 167, pp. 81–85. https://doi.org/10.1016/j.scriptamat.2019.03.031

[152] M.Yu. Gutkin, A.L. Kolesnikova, I.S. Yasnikov, A.A. Vikarchuk, E.C. Aifantis and A.E. Roma-nov, *Fracture of hollow multiply-twinned parti-cles under chemical etching*, European Journal of Mechanics – A /Solids, 2018, vol. 68, pp. 133–139. https://doi.org/10.1016/j.euromechsol.2017.11.004

[153] A.L. Kolesnikova and A.E. Romanov, *For-mation of mismatched layers in pentagonal na-norods*, Physica Status Solidi, 2007, vol. 1, no. 6, pp. 271–273. https://doi.org/10.1002/pssr.200701204

[154] L.M. Dorogin, S. Vlassov, A.L. Kolesnikova, I. Kink, R. Lõhmus and A.E. Romanov, *Crystal mismatched layers in pentagonal nanorods and nanoparticles*, Physica Status Solidi B, 2010, vol. 247, pp. 288–298. https://doi.org/10.1002/pssb.200945385

[155] L.M. Dorogin, A.L. Kolesnikova and A.E. Ro-manov, *Misfit layer formation in icosahedral na-noparticles*, Technical Physics Letters, 2008, vol. 34, no. 9, pp. 779–781. https://doi.org/10.1134/S1063785008090198

[156] M.Yu. Gutkin and S.N. Panpurin, *Spontaneous formation and equilibrium distribution of cylin-drical quantum dots in atomically inhomogene-ous pentagonal nanowires*, Journal of Macro-molecular Science, Part B: Physics, 2013, vol. 52, no. 12, pp. 1756–1769. https://doi.org/10.1080/00222348.2013.808929

[157] M.Yu. Gutkin and S.N. Panpurin, *Equilibrium en-sembles of quantum dots in atomically inhomoge-neous pentagonal nanowires*, Physics of the Solid State, 2014, vol. 56, no. 6, pp. 1187–1194. https://doi.org/10.1134/S1063783414060134

[158] Y. Ding, X. Sun, Z.L. Wang and S. Sun, *Misfit dislocations in multimetallic core-shelled nano-particles*, Applied Physics Letters, 2012, vol. 100,

no. 11, art. no. 111603.
https://doi.org/10.1063/1.3695332

[159] N. Bhattarai, G. Casillas, A. Ponce and M. Jose-Yacaman, *Strain-release mechanisms in bimetallic core-shell nanoparticles as revealed by Cs-corrected STEM*, Surface Science, 2013, vol. 609, pp. 161–166.
https://doi.org/10.1016/j.susc.2012.12.001

[160] S. Khanal, G. Casillas, N. Bhattarai, J.J. Velázquez-Salazar, U. Santiago, A. Ponce, S. Mejia-Rosales and M. José-Yacamán, *CuS₂-passivated Au-core, Au₃Cu-shell nanoparticles analyzed by atomistic-resolution Cs-corrected STEM*, Langmuir, 2013, vol. 29, no. 29, pp. 9231–9239.
https://doi.org/10.1021/la401598e

[161] S.A. Krasnitckii, M.Yu. Gutkin, A.L. Kolesnikova and A.E. Romanov, *Formation of a pore as stress relaxation mechanism in decahedral small particles*, Letters on Materials, 2022, vol. 12, no. 2, pp.137–141.

[162] N.M. Vlasov and I.I. Fedik, *Diffusion-induced relaxation of residual stresses*, Doklady Physics, 2000, vol. 45, no. 11, pp. 623–626.
https://doi.org/10.1134/1.1333871

[163] N.M. Vlasov and Y.G. Dragunov, *Phase transformations in pentagonal nanocrystals*, Technical Physics, 2013, vol. 58, no. 2, pp. 218–222.
https://doi.org/10.1134/S1063784213020266

[164] N.M. Vlasov and V.A. Zaznoba, *Kinetics of migration (deposition) of fission products and interstitial impurities to sinks with different singularities*, Physics of the Solid State, 2014, vol. 56, no. 3, pp. 518–521.
https://doi.org/10.1134/S1063783414030354

[165] A.E Romanov and G.G. Samsonidze, *Diffusion in the elastic field of a wedge disclination*, Soviet Technical Physics Letters, 1988, vol. 14, no. 14, pp. 585–586.

[166] A.S. Khramov, S.A. Krasnitckii and M.Yu. Gutkin, 2022, to be submitted to Journal of Materials Physics and Mechanics.

[167] I. Tsagrakis, I.S. Yasnikov and E.C. Aifantis, *Gradient elasticity for disclinated micro crystals*, Mechanics Research Communications, 2018, vol. 93, pp. 159–162.
https://doi.org/10.1016/j.mechrescom.2017.11.007